This student is registered as dyslexic / dyspraxic with UCL Student Disability Services.

Please refer to Guidance for Academic Staff: Assessment of the work of students with specific learning difficulties – Dyslexia / Dyspraxia

http://www.ucl.ac.uk/disability/info-for-staff/dyslexia-marking-guidelines

Noise Suppression in a Raman Quantum Memory

Thomas Muir Hird

Centre for Doctoral Training in Delivering Quantum Technologies

University College London

Supervisors: Dr Dylan Saunders and Professor Ian Walmsley

Declaration

I, Thomas Muir Hird, confirm that the work presented in this thesis is my own. Where information has been derived from other sources, I confirm that this has been indicated in the thesis.

Abstract

A significant cornerstone of photonic based quantum technologies has been identified as a quantum memory; a device which can store and retrieve an arbitrary quantum state at the single photon level. The development of such a memory would allow the creation and development of a large number of quantum technologies ranging from the ability to synchronise processing steps in an optical based quantum computer, to the construction of a quantum repeater which would allow for perfect transmission of quantum states over arbitrarily long distances. This report reviews optical quantum memories and reports on recent developments in delivering a room temperature memory for broadband photons. A novel scheme to suppress four-wave mixing is simulated, based on equations derived to describe the physics of the memory interaction. Finally the experimental arrangement to test the suppression method is described and future developments in this field are considered.

Contents

List of Figures

Introduction

Quantum technologies offer the ability to surpass the current classical limits in applications spanning simulation, metrology, communication and computation. Technology which can utilise features such as entanglement and superposition have been shown to be able to perform certain types of computation exponentially quicker than possible with current, conventional technologies[1]. Furthermore, within the rapidly developing field of Quantum Information Processing (QIP) exists the possibility for completely secure communication and the transfer of quantum states[2].

Qubits have been realised using a number of different media including super-conductors, quantum dots and donor ions in silicon, but to-date there is no single architecture which satisfies all of the requirements in implement quantum technologies.For the transfer of quantum information, optical-frequency photons make a promising "flying qubit" since they travel at the speed of light and interact weakly with the environment. They are also noise free at room temperature and possess multiple degrees of freedom such as spatial/temporal modes and polarisation. Single qubit unitaries can be implemented with simple linear optics such as waveplates, phase-plates and beam-splitters; however due to weak photon-photon interaction two-qubit gates are difficult to implement deterministically which inherently limits the size currently possible for photonic networks.

The solution to this scaling problem is to develop a multiplexed architecture whereby probabilistic operations are performed repeatedly until successful, and the successful occurrences combined. It has been shown that the advent of a quantum memory, which could store and faithfully retrieve photons on-demand, would allow significant development in liner optical quantum computing (LOQC) with multiplexing and in the building of quantum repeaters for long distance quantum communication[3].

Such motivation has spurred a significant body of research into this field with a number of proposed implementations for a photonic quantum memory[4]. One such implementation is the Raman memory protocol which is currently being studied at Oxford University and offers the possibility for room-temperature storage of GHz-bandwidth pulses for microsecond time-scales[5] - properties particularly advantageous for applications in temporal multiplexing[6]. Current implementations of the memory suffer from four-wave mixing noise[7] but this may be negated with the development of a new noise-suppression proposal. In this thesis we model this noise suppression mechanism numerically, and discuss an experimental set-up to investigate the proposal further.

This thesis is arranged as follows: Chapter 1 reviews the current state of the art of quantum memories detailing potential applications and comparing proposed implementations. Chapter 2 derives the equations that govern the Raman memory protocol and models a proposed noise suppression scheme numerically while Chapter 3 details how this proposal may be investigated experimentally. Finally, Chapter 4 will outline future steps for development of a Raman memory and draw the final conclusions of the thesis.

Chapter 1

Review on Quantum Memories

This chapter <mark>will aim</mark> to evaluate the current state of the art of quantum memories reviewing key applications in Section 1.2 and discussing how they may be used in currently emerging technologies. Section 1.3 <mark>will discuss</mark> the principle behind a number of proposed implementations as well as providing insight into the current limitations and challenges in this field.

1.1 Background

A quantum memory can be described as "a system which is able to store and retrieve a quantum state on-demand". This has particular significance in LOQC as they offer a potential scheme with which to implement photon synchronization and temporal multiplexing following probabilistic operations. These applications will be discussed in detail in the following section.

All memories where the storage and retrieval of photons is considered have an associated efficiency η which is the ratio of energies between the output and input signals. In the case of single photon storage the efficiency is analogous to the probability of retrieving a photon given one was sent into the memory. Efficiency may be further decomposed into *read-in* and *read-out* efficiencies which may be written as:

$$\eta_{read-in} = 1 - \frac{\mathcal{E}_{trans}}{\mathcal{E}_{input}}; \qquad \eta_{read-out} = \frac{\mathcal{E}_{ouput}}{\mathcal{E}_{input} - \mathcal{E}_{trans}} \qquad \eta_{total} = \frac{\mathcal{E}_{output}}{\mathcal{E}_{input}} = \eta_{read-in} \times \eta_{read-out}$$

(1.1)

<mark>where $\mathcal{E}$ is the energy associated with that pulse,*input/trans* refers to signal that is input into/transmitted through the memory and *output* refers to signal that is retrieved from the memory.</mark> These will have greater significance when the beam splitter picture is considered in Section 1.3.

For memories used in temporal multiplexing a critical figure of merit is given by the product ηB where η is the total memory efficiency (previously η_total) and B is the time-bandwidth product defined as $B = \tau\delta$ where τ is the lifetime of the memory and δ is the acceptance bandwidth of the stored signal. Consideration of a signal's bandwidth has further significance in computation where it is desirable to operate at a high repetition rate with short pulses which (due to the Fourier transform relationship between frequency and pulse length) implies large signal bandwidth.

There is also a requirement on a quantum memory that the recovered state be the same as (or close to) the state we stored. To quantify this we consider the fidelity $\mathcal{F}$ which can be considered

as the overlap between two quantum states and can is given by $\mathcal{F} = \left| \text{Tr}(\sqrt{\sqrt{\rho_{in}}\rho_{out}\sqrt{\rho_{in}}}) \right|^{2}$[8, 9] where $\rho_{in/out}$ are the density matrices of the stored/recovered state. A memory could only be considered quantum if it surpassed the maximum recovered fidelity from a classical device. One could imagine a classically stored measurement of the target state, and the preparation of a new state based on the results. This would on average yield a fidelity of $2/3$[10], hence for a memory to be considered quantum it must exceed this value.

The fidelity is also closely linked to the noise of the retrieved state; for the storage of weak coherent states the single to noise ratio (SNR) can be used. In the case of true single photon storage, zero added intensity noise would be the ability to store photons with a second order correlation $g^{(2)} = 0$ and retrieve them with the same $g^{(2)}$ whilst added phase noise or modification of the state would induce other errors (as a reduction in fidelity or increased distinguishablity between what were previously identical photons). One could imagine an experiment where one of two indistinguishable photons was stored and retrieved from the memory and interferred with the other; their distinguishablity could be compared using the Hong-Ou-Mandel effect[1][11].

1.2 Applications

The two applications which have been driving factors in the development of quantum memories are applications of *temporal multiplexing* and the realisation of a *quantum repeater*. Multiplexing provides a solution to the scaling problem in photonic quantum networks as well as providing a means to generate deterministic single photons which forms a constituent part in universal quantum computing proposals[12] (as well as in some quantum repeater proposals[13]).

The transfer of arbitrary quantum states can be achieved between parties sharing an entangled system. The problem lies in the distribution of this entanglement; current optical fibres can reliably transfer quantum states short distances but are currently limited by photon losses in the fibre and decoherence. The solution, as proposed by Briegel et al. [14], is to have the transmission length divided into segments separated by nodes of quantum repeaters. The crucial finding of Briegel was that the decay of the information with a repeater architecture could scale polynomially and not exponentially with distance. The objective of the repeater is to perform entanglement swapping with an adjacent mode such that two nodes further apart then become entangled. This is again an inherently probabilistic process and as such quantum memories are required so a node can wait until entanglement has been heralded in an adjacent one.

It is worth mentioning at this point that the potential applications go beyond the two explored in detail below. For example the possibility for entanglement enhanced sensing whereby the storage of entanglement is used as a resource with applications in improving the precision of quantum sensors[4, 15].

1.2.1 Temporal Multiplexing

As outlined above, temporal multiplexing is the synchronisation of successful probabilistic outcomes which are repeatedly attempted[16]. Synchronisation is achieved by storing the heralded outputs of successful operations inside a quantum memory and synchronising the output[17]. We now consider the improvement a quantum memory provides to the significant issue of single photon synchronisation.

---

[1]The Hong-Ou-Madnel effect is discussed in detail in Section 4.1.2

The optical pumping of a non-linear $\chi^{(2)}$ crystal provides a means to produce heralded single photons via spontaneous parametric down-conversion (SPDC)[18]. This process is stimulated by random vacuum fluctuations and is therefore an inherently probabilistic process. For use as a single photon source it is a necessity that SPDC sources be operated with a low probability of production $p \ll 1$ (typically $p \sim 0.01$)[19] such that the likelihood of multi-photon events is negligible.

The probability of producing N single photons from N sources simultaneously scales exponentially with p^N; the production of 10 simultaneous photons is of order 1 in 10^{20}. Figure 1.1 (a) shows how memories can be used to solve this issue with N memories and N probabilistic single-photon sources. Once $N-1$ memories are storing single photons they are all read-out on demand, heralded by the emission of the Nth, yielding an N-fold coincidence. It has been shown that the rate of this coincidence is dependent upon time-bandwidth product B and efficiency η[6].
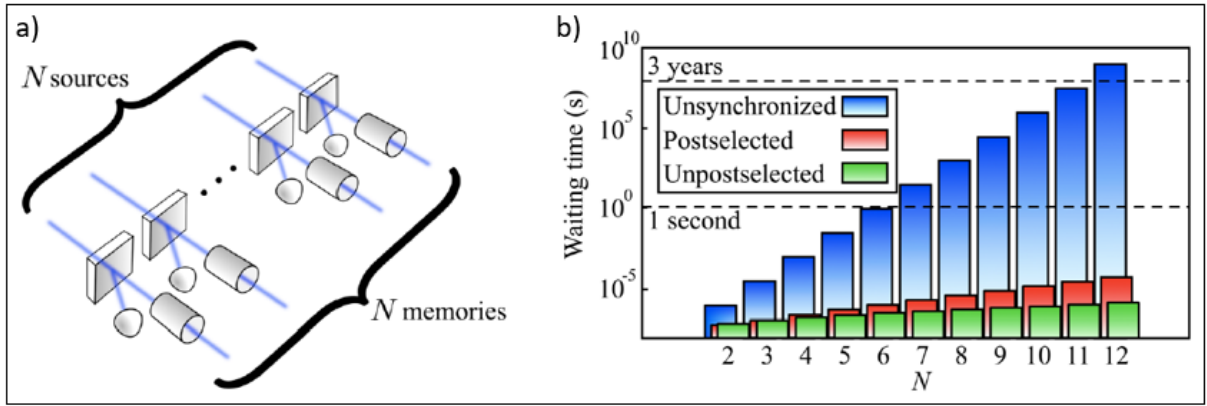
Figure 1.1: a) Schematic for a scheme to produce an N-photon coincidence using N single photon sources and N quantum memories. b) Average waiting times for N-photon coincidences with a threshold fidelity of 90% under three conditions. Blue is using unsynchronised sources whilst red and green show waiting times with the inclusion of a quantum memory with a time-bandwidth product $B = 1000$. Red shows post-selected photons from a memory with efficiency $\eta_{total} = 56\%$ and green has $\eta_{total} = 99\%$. Figure from [6]

Figure 1.1 (b) shows the potential reduction in waiting time for a synchronised N-photon event with the inclusion of a quantum memory with $B = 1000$. The principle figure of merit for this application is the time-bandwidth product and demonstrates significant improvement achieved with a relatively modest efficiency. This example displays how memories may be used as a solution to scalability for non-deterministic processes in quantum photonic networks.

1.2.2 Quantum Repeater

The idea behind a quantum repeater is to allow entanglement to be "swapped" by a measurement such that entanglement is transferred to photons which are further apart.

Figure 1.2 shows a simple schematic for a quantum repeater node consisting of an EPR source for producing entangled photons and quantum memories. If the distance between 1 and 2 is too great that transmission of quantum information is not possible because of fibre loss then the distance can be reduced by the addition of a quantum repeater. The photons are stored in the memories until the adjacent memory has also stored a photon. The pair can be recalled on

demand and by way of a Bell-state measurement the entanglement is projected onto another pair of states (be they photons or photons stored in memories in other nodes). The result of the Bell-State measurement can be seen explicitly when the DLCZ protocol is examined in Section 1.3.4 and the extension of the set-up shown in Figure 1.2 is simple, by just adding subsequent nodes the distance between 1 and 2 can be come arbitrarily large.
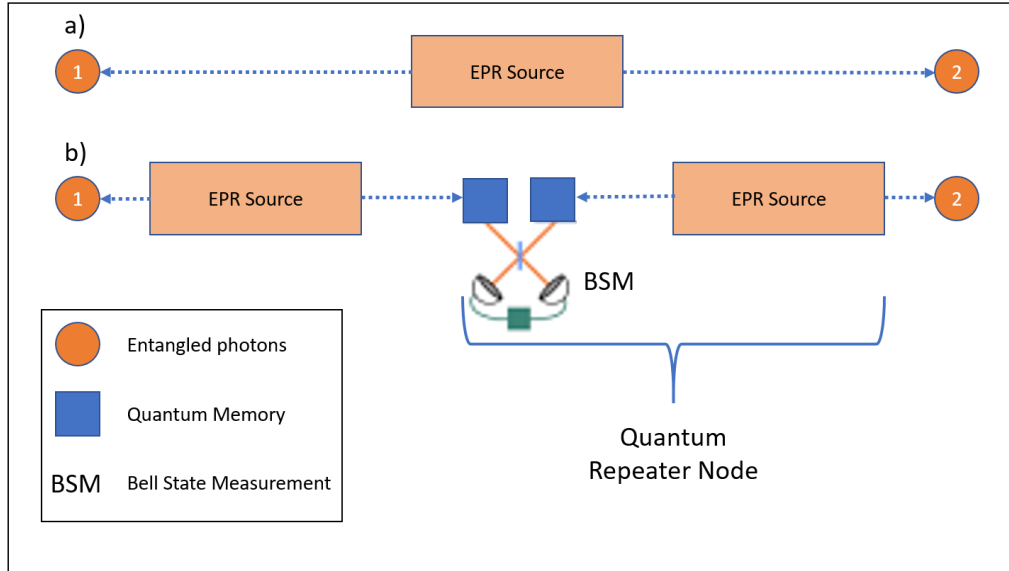
Figure 1.2: Showing how the distance travelled by a photon to create entanglement between two parties (1 and 2) reduces with the addition of a quantum repeater node (b). The BSM causes the entanglement to be projected such that 1 and 2 now share a maximally entangled pair.

The realisation of a quantum repeater would fill the gap between local processing (such as that performed by a quantum computer) and the long distance communication of quantum information (the basis of a *Quantum Internet*[20]). There is little doubt therefore that the development of a quantum repeater (and by extension, quantum memories) is one of significant importance.

1.3 Implementations

There are a number of possible physical systems with which quantum memories can be realised with protocols developed each with its own set of advantages and disadvantages. In this section I will review the physical processes behind a number of proposals and discuss limitations they may have.

The simplest way one could imagine storing a photon would be simply to extend its optical path length, possible in free space[21], a fibre or a cavity[22], where active switching could be used for retrieval. However these systems are currently limited by loss (switching loss, fibre loss or intracavity loss) which means that they are not currently suited for application in larger scale quantum networks[23]. TALK ABOUT [24].

To store light in matter requires a strong coupling which can be achieved by use of a cavity. One could then imagine storing a transition in an isolated atom[25], this however severely restricts the bandwidth it is possible to store. The other method to increase the coupling is to then use an ensemble of atoms - reducing the technical overhead in fabricating a cavity. In this regime the signal is stored as a collective excitation of the ensemble.

1.3.1 EIT

The interaction between optical fields and multilevel atoms can lead to quantum interference that can dramatically alter the optical properties of a medium[26]. One such example is the non-linear effect Electromagnetically Induced Transparency (EIT) where Fano interference between transition pathways creates a transparency window for frequencies surrounding a transition.

This effect can be seen in atoms with a Λ-level energy structure as seen in Figure 1.3 (a) where two ground states ($|1\rangle$ and $|3\rangle$)are coupled to a single excited state ($|2\rangle$). Coupling is achieved by a strong control field and a weak signal (or probe) field. Absorption of the probe can occur by the process $|1\rangle \rightarrow |2\rangle$ and by $|1\rangle \rightarrow |2\rangle \rightarrow |3\rangle \rightarrow |2\rangle$. The amplitudes for these transitions interfere destructively and hence the probe is not absorbed - Figure 1.3 (b). The change in absorption is accompanied by a large change in dispersion, which in-turn results in a dramatic change to the group velocity of the signal $v_g = \mathrm{d}\omega/\mathrm{d}k = c/(n + \omega \mathrm{d}n/\mathrm{d}\omega)$.
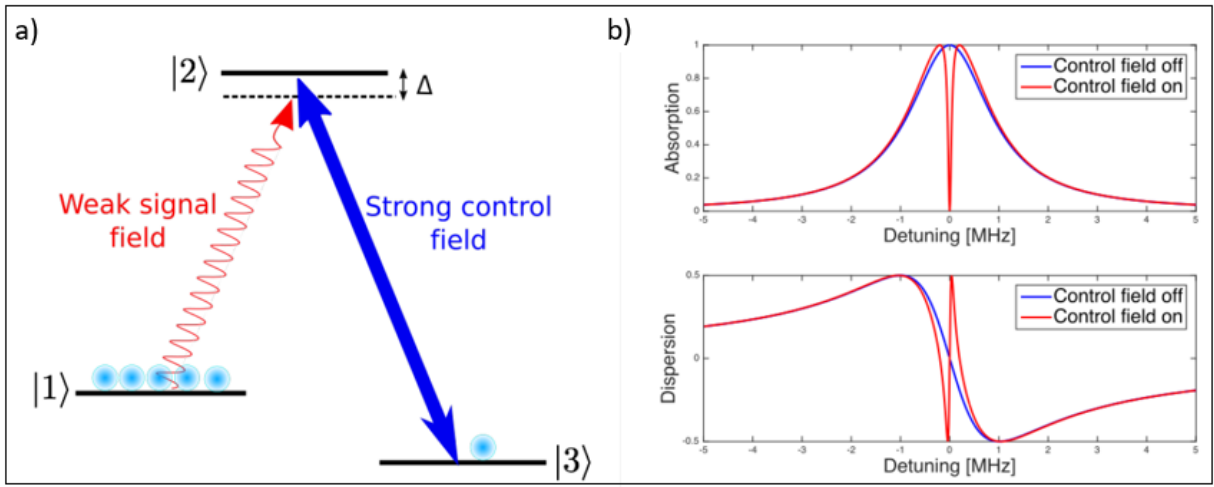
Figure 1.3: (a) Λ energy level structure used in Electromagnetically Induced Transparency with a strong control and weak signal field coupling two ground states to an excited level. (b) Shows the absorption and dispersion as a function of signal detuning from the $|1\rangle \rightarrow |2\rangle$ transition with (red) and without (blue) the bright control field. Figure from [27]

To use this process as a memory follows the following procedure:

1. The ensemble of atoms are prepared in the state $|1\rangle$ and the control field field is applied. The signal is incident on the ensemble and propagates through (slowly) without loss.

2. The control field is adiabatically reduced to zero, bringing the signal to a halt within the ensemble ($v_g = 0$). The quantum state of the signal is transferred to a ground state coherence (or *spin-wave*) within the ensemble of M atoms with the form:

$$|\Psi\rangle = \sum_j^M \psi_j e^{i\Delta k z_j} |0_1 0_2 .... 1_j ... 0_M\rangle \tag{1.2}$$

where z_j is the position of the j_{th} atom and Δk is the difference between the wave-vectors of the control and signal fields[23]. The amplitudes ψ_j correspond to the interaction strength the jth atom feels.

3. Increasing the control field adiabatically results in the retrieval of the signal from the ensemble.

Using EIT as a memory was first proposed by Fleischhauer and Lukin [28] and was realised by Philips et al the following year [29] using rubidium vapour. Since then it has been developed and implemented using both atomic ensembles[30] and in solid state media[31]. Two key limitations of EIT memories are 1) the possible signal bandwidth; this is typically of order MHz[32] and 2) four-wave mixing noise (the process for which is discussed in detail in the following chapter) is inherent to the system, limiting its applications in single photon storage. There are however proposals to use the orbital angular momentum (OAM) degree of freedom in photons as qubits, and EIT memories have been shown to store photons with OAM, expanding their potential applications in this field[33, 34].

1.3.2 Raman Memory

The Raman interaction describes the inelastic scattering of a photon from a transition. This linear two-photon process is mediated by a second-order dipole interaction[23, 35] and has two possible outcomes: The scattered photon can have a frequency lower than or greater than the absorbed photon. These processes are known as Stokes and anti-Stokes respectively.

Like EIT the Raman memory protocol makes use of the Λ level system shown in Figure 1.4 however differs by the large detuning Δ of both the signal and the control from the excited state $|2\rangle$. The storage process is very similar to that of the EIT protocol but differs with some small subtleties.

1. Again the atomic ensemble are prepared in $|1\rangle$ and the control field and signal field are applied. The control field is detuned from the $|2\rangle \leftrightarrow |3\rangle$ by the same amount Δ as the signal is detuned from the $|1\rangle \leftrightarrow |2\rangle$ transition, such that they are in two-photon resonance.

2. The quantum state of the signal is transferred by Raman scattering to the same spin-wave coherence given by Equation 1.2. Retrieval of the signal field occurs by the re-application of the control field and the signal is re-emitted as a Stokes photon.

3. Because the signal is not restricted by a transparency widow the signal can be very broadband with its bandwidth limited by only the control's bandwidth and the need to optically address the ground states individually. This is determined by its ground state splitting Δ_g and if the hyperfine levels in the ground-state of Caesium are used as $|1\rangle$ and $|3\rangle$ then $\Delta_g = 9.2GHz$ and the acceptance bandwidth can be order of gigahertz[7].
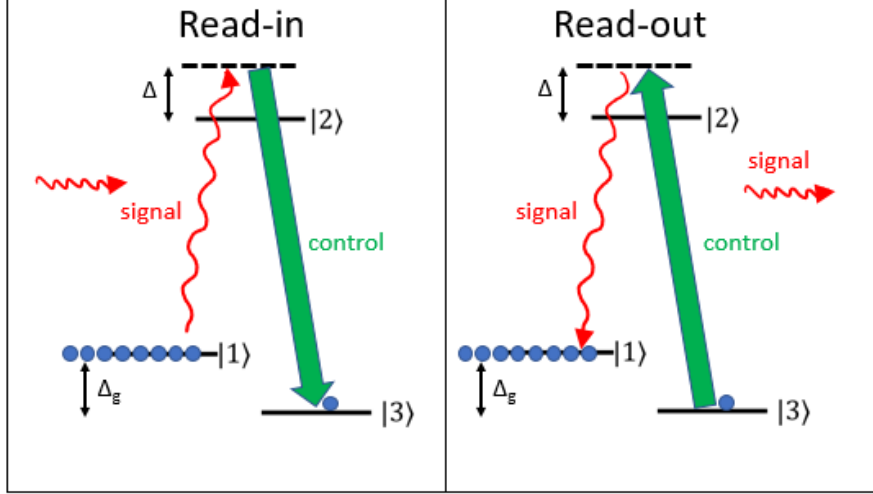
Figure 1.4: Energy level structure for the read-in and read-out stages of the Raman memory protocol showing the frequencies of the signal and control fields.

The GHz possible bandwidth stored in the Raman memory, combined with the possible storage time of greater than microseconds yields a time-bandwidth product > 1000, meeting the requirement discussed above for temporal multiplexing. The Raman memory protocol was first demonstrated in 2009 [36] with a bandwidth of 1.2GHz and total efficiency of 15%. A complete discussion of previous experiments using the Raman memory in Caesium will be discussed in Section 3.1 but implementations have seen $B \sim 4000$ and noise suppressed to a level almost allowing single-photon storage whilst maintaining its quantum statistics. Discussions of noise suppression in this memory implementation with hot caesium vapour will form much of the following two chapters. Other significant results of the Raman protocol come from the storage of THz bandwidth photons in molecules[37] and bulk diamond[38] which demonstrate the capacity of the Raman protocol to store high bandwidth photons although the memory lifetime is prohibitively short in these demonstrations ($\sim$1ns in hydrogen molecules, $\sim$ 3.5ps in diamond). Finally the Raman memory protocol has also recently been demonstrated with the storage of polarisation entanglement using a cold Rubidium ensemble where selection rules can be used to reduce four-wave mixing, this does however limit the bandwidth to $\sim$ 140 MHz but represents a important milestone with the storage of entanglement[39].

Another factor which separates the Raman memory from other memories is the fact that the un-stored signal is not absorbed (because it is so far detuned) but rather transmitted. This combines with the description of the Raman memory by way of a beam-splitter Hamiltonian:

$$\mathcal{H}_{BS} = C_s \hat{s} \hat{b}^\dagger + h.c. \qquad \text{where} \quad C_s \propto \sqrt{N} \left(\frac{\Omega}{\Delta} \right). \qquad (1.3)$$

Here $\hat{s}, \hat{b}$ are annihilation operators for the signal and spin-wave coherence respectively and C_s is the coupling constant for the Raman interaction, proportional to the Rabi frequency of the control (Ω), the square root of the number of atoms in the interaction, N, and inversely proportional to the detuning Δ. The memory process may then be thought of as two successive light-matter beam splitters where the read-in and read-out efficiencies correspond to reflectivities - a correspondence that has potentially novel applications since beam splitters play such an instrumental role within LOQC.

1.3.3 Photon-Echo Memories

EIT and the Raman protocol form two sides of the same coin - Λ-level schemes in which the signal is mapped adiabatically to a spin-wave coherence without the upper level ever being populated. There do exist a number of alternative memory protocols which borrow from the Hanh echoes used in NMR[40] - these are *Photon-Echo Memories*. The principle behind it is simple: a $\pi/2$ signal pulse is applied to a system of 2 level atoms initialised in the ground state $|1\rangle$. The result is a coherent superposition to the state:

$$|\psi\rangle = \frac{1}{\sqrt{2}}(|1\rangle + e^{i\phi}|2\rangle) \tag{1.4}$$

In practice however this process will suffer from some inhomogeneous broadening which could be from a velocity distribution in warm vapours or strain fields in solid states, all atoms will dephase at a different rates resulting (after time τ) in the state:

$$|\psi\rangle = \sum_j \frac{1}{\sqrt{2}}(|1\rangle + e^{i(\delta_j \tau + \phi)}|2\rangle) \tag{1.5}$$

where δ_j the difference in detuning felt by each atom labelled by j. If a π pulse is then applied and the atoms dephase after a further time τ then the dephasing already experienced is effectively cancelled and results in only a global phase. This re-phasing causes an *echo*, and the signal is re-emitted as the atoms return to the ground state.

$$|\psi\rangle \xrightarrow{\pi \, pulse} \sum_j \frac{1}{\sqrt{2}}(e^{i(\delta_j \tau + \phi)}|1\rangle + |2\rangle) \xrightarrow{t=\tau} \sum_j \frac{e^{i\delta_j \tau}}{\sqrt{2}}(e^{i\phi}|1\rangle + |2\rangle) \xrightarrow{signal} |1\rangle \tag{1.6}$$

The optical π pulse is however not well suited to photonic memories as can lead to severe problems due to spontaneous emission[23]. It is therefore preferable manipulate the re-phasing via control of the broadening process, resulting in a number of proposals summarised below.

Controlled and Reversible Inhomogeneous Broadening (CRIB) and Gradient Echo Memories (GEM) are schemes where an inhomogeneous broadening to the $|1\rangle \leftrightarrow |2\rangle$ transition is achieved by applying an electric or magnetic field which induces a Stark or Zeeman splitting. For example in CRIB the state of the ensemble of M atoms involved in the interaction after absorbing the signal is[23]:

$$|\psi\rangle = \sum_j \psi_j e^{i\delta_j t} e^{ikz_j} |0_1..1_j...0_M\rangle \tag{1.7}$$

where k is the wavevector of the signal and δ_j is again the detuning felt by the jth atom caused by a transverse filed. Here, as the dephasing is due to the external field, by reversing the direction of the applied field after time τ causes the detuning felt by each atom to reverse and hence the signal is re-emitted by the echo. GEM differs to CRIB in the direction of the field gradient, where it is applied along the direction of propagation of the signal. This causes the detuning to vary across the sample, essentially encoding the frequencies of the signal to a spatial location. This prevents re-absorption during the read-out phase, maximising (read-out) efficiency.

The final photon-echo method discussed is most similar to CRIB but with some subtleties where it "burns" spectral holes into an inhomogeneously broadened transition to create an Atomic Frequency Comb (AFC) . In contrast to CRIB however the inhomogeneous broadening does not have to be reversible, it can be due to (for example) the broadening experienced in rare-earth

doped crystals[41]. The result of this is the creation of a set of energy levels equally spaced by Δ (see Figure 1.5 (c)) which induce dephasing which (like in CRIB) must be re-phased to re-emit the signal. Unlike CRIB however, because of the periodic nature of the energy spacing re-phasing will occur (periodically) after a time $(2\pi/\Delta)$ without any change in fields.

The benefit of AFC compared to CRIB is in the ability to make use of inhomogeneous broadenings which are unsuitable for CRIB. In CRIB atoms not in a narrow resonance need to be removed from the interaction by optical pumping, whilst in AFC they need to be removed from not being in N narrow resonances which spans much fewer atoms. It is important to note that AFC in two-levels cannot be read-out on demand, but all the photon-echo processes described can in principle benefit from the addition of a third level using the Λ configuration. The excitation may then be mapped to the third level just as in EIT and Raman to increase storage time and allow on-demand retrieval for AFC. The mapping to the third level is the same, transfer is completed with a bright control pulse, as shown in Figure 1.5.
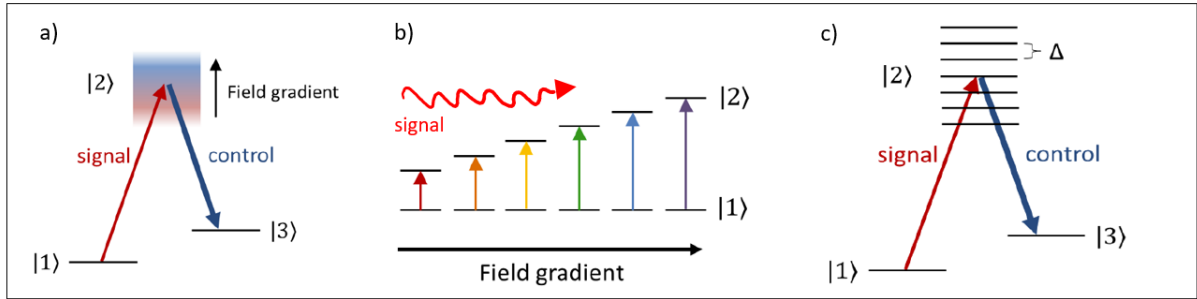
Figure 1.5: Energy level structure for the read-in procedures of a) CRIB b) GEM and c) AFC. In CRIB and GEM the field gradient applied must be reversed for read-out whilst this is not the case in AFC. Figures from [23].

1.3.4 DLCZ

The final implementation of a memory was touched briefly on in Section 1.2.2 and is distinct from the others in that the memory storage is heralded by the emission of a photon. The scheme also provides a natural way for entanglement to be transferred to spatially separated nodes - the constituent part for a quantum repeater and was conceived by Duan, Lukin, Cirac and Zoller in 2001[2]. The so called DLCZ protocol makes use of the Raman scattering seen in a atomic ensembles (Figure 1.4) except that in this case the write pulse is bright, and emits a Stokes photon which heralds the storage of the excitation. Read-out is then achieved with a resonant pulse and the *signal* is re-emitted as an anti-Stokes photon. Note this *signal* should not be thought of in the same way as signal in the previous memories - in this case it is a herald that the excitation is no longer present.

Figure 1.6 (b) shows how this scheme may then produce a Bell-like state: applying write pulses to two ensembles A and B and having their heralded Stokes photons incident on a beam-splitter combined with a single detection event would produce the state $|\psi\rangle_{AB} = \frac{1}{\sqrt{2}}(|0\rangle_A |1\rangle_B + |1\rangle_A |0\rangle_B)$ where $|1\rangle_J$ and $|0\rangle_J$ represent if ensemble J is storing an excitation or not.

Figure 1.6: a) Energy level structure for the read-in and read-out Raman scattering interaction in the DLCZ protocol. b) Entanglement is created between two ensembles by having t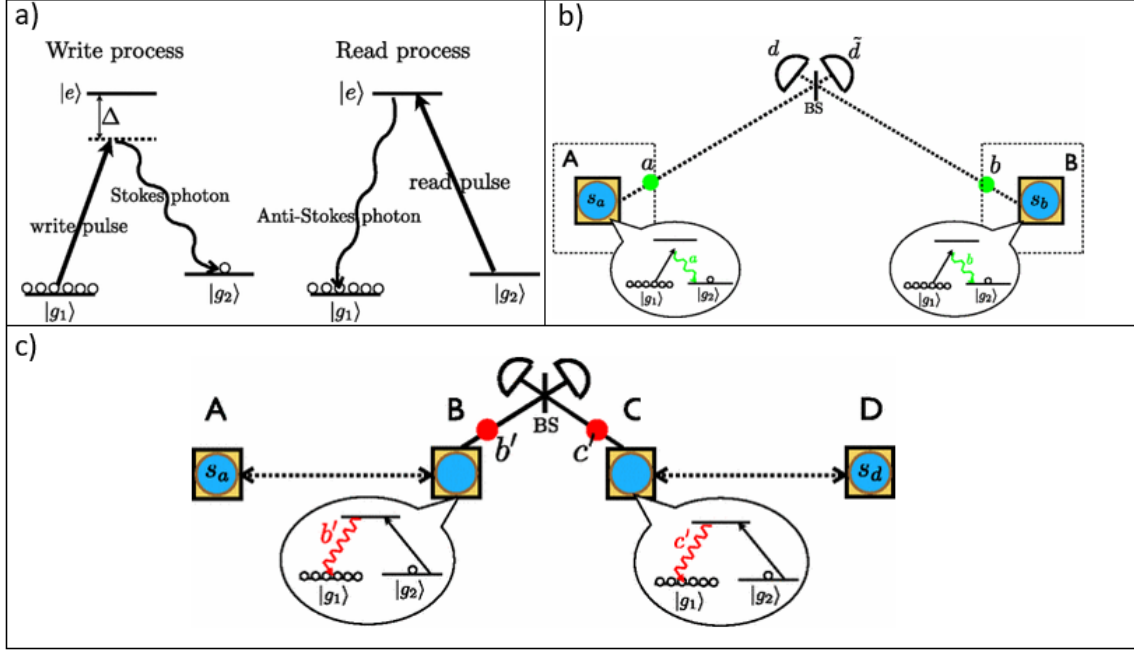he emitted Stokes photon incident on a beam-splitter: a single detection event places creates a superposition of the excitation being in A or B. c) The same principle may be used to project the entanglement onto A and D by reading-out B and C and measuring a single detection event. Figures from [42].

The natural extension of this is to combine two of these Bell states as shown in Figure 1.6 (c) where we start with the state:

$$|\psi\rangle_{ABCD} = \frac{1}{\sqrt{2}}(|0\rangle_A |1\rangle_B + |1\rangle_A |0\rangle_B) \otimes \frac{1}{\sqrt{2}}(|0\rangle_C |1\rangle_D + |1\rangle_C |0\rangle_D)$$

$$= \frac{1}{2}(|0101\rangle + |0110\rangle + |1001\rangle + |1010\rangle) \tag{1.8}$$

Simultaneous read-pulses onto the ensembles B and C are applied with the output anti-Stokes photons (b' and c' in the figure) incident on a beam-splitter and two detectors. A single detection result signifies that one ensemble has been read-out but gives no information as to which one - this can be thought as a projection onto the subspace: $\frac{1}{\sqrt{2}}(|0\rangle_B |1\rangle_C + |1\rangle_B |0\rangle_C)$ which results in:

$$|\psi\rangle_{AD} = \frac{1}{\sqrt{2}}(\langle 01|_{BC} + \langle 10|_{BC})|\psi\rangle_{ABCD} \tag{1.9}$$

$$= \frac{1}{\sqrt{2}}(|0\rangle_A |1\rangle_D + |1\rangle_A |0\rangle_D) \tag{1.10}$$

Hence a Bell-state has been created between (in principle) spatially separated ensembles A and D (note the normalisation factor in equation 1.9 has been omitted). This is precisely the operation desired in Section 1.2.2, and could form the basis of a quantum repeater network[42]. It is important to note this is an absorbative memory where the memory stores information of a quantum excitation as opposed to a quantum state.

1.4   Comparison and Outlook

The search for an ideal quantum memory is not an easy one, as evidenced by the number of memory protocols. Moreover these protocols can be implemented in a a number of different media which I shall discuss the benefits of in broad terms. I shall exclude from this discussion both the *delay-line memory* and the *DLCZ* protocol as these can be characterised as different class compared to the absorbative memories discussed.

The three primary different mediums in which memory protocols are implemented are: 1) Warm vapours ensembles (such as caesium[43] and rubidium[44,45]), 2) Cold atomic ensembles (such as Caesium[33]), and 3) Rare earth ions in solids (such as erbium doped crystal[46]) although there are others such as single atoms in an optical trap[47].

- EIT in warm Rb -($\eta = 0.1, 0.05$) ($\mu_1 = 1, 0.17$), $B \approx 20, 5ns, \mu s$ [44][45]

- EIT in cold Cs - ($\eta = 0.15, \mu_1 = 0.06, B = 30, 0.5\mu s, 15\mu s$ [33]

- EIT rydberg - $500ns$[48]

- Raman Diamond - ($\eta = 0.09, \mu_1 = 0.04, B = 13, 250fss, 3.5ps$)[49]

- Raman Cs, H, Cavity

- AFC ($\eta = 0.05, \mu_1 = 0.2, B = 500, 1\mu ss, 500\mu s$) [50]

- GEM ($\eta 0.86, 7\mu s, 600\mu s$)[51]

It might be useful here in the comparison to build a table that compares the various benchmarks and which memories are suited to them. Briefly compare:

Warm Vapour Cold Atoms Solid State (Rare Earths)

with their advantages and disadvantages?

As the discussion is protocols, then platforms. then which is best for which application (local vs global).

Chapter 2

Theory

The rest of this thesis concerns itself with the Raman memory protocol implemented in warm atomic caesium vapour.Combining broadband storage, high time-bandwidth products, on-demand recall capabilities and room temperature operation, the Raman memory is particularly well-suited for temporal multiplexing tasks. This chapter will outline existing theory of the Raman memory protocol and discuss the sources of noise inherent to the protocol. By considering the coherences in Raman's Λ-level system I am able to construct and simulate the equations of motion for the system and emulate the read-in, storage, and retrieval interaction of the memory. By extension this approach also enables analysis of the noise processes inherent to the memory, providing the ability to consider a novel noise-suppression scheme.

2.1 Equations of motion

This derivation follows and builds on that from references [23,27,35] and differs by the inclusion of an anti-Stokes field. Consider an ensemble of Λ-type atoms which have ground states $|1\rangle$ and $|3\rangle$, and an excited state $|2\rangle$. As shown in Figure 2.1, coupling between the ground and excited states is achieved by a strong control field $\mathbf{E_c}$, and weak signal $\mathbf{E_s}$ with central frequencies ω_c and ω_s respectively. The existing additional coupling shown is the result of unwanted anti-Stokes scattering and is described by electric field $\mathbf{E_a}$ with central frequency ω_a.

The total Hamiltonian for this light-matter interaction may be written as the sum of 3 constituent Hamiltonians: that of the atom ($\hat{H}_A$), the free-field Hamiltonian ($\hat{H}_L$) and of the electric-dipole interaction ($\hat{H}_{ED}$).

$$\hat{H} = \hat{H}_A + \hat{H}_L + \hat{H}_{ED} \tag{2.1}$$

The atomic Hamiltonian may be diagonalised in the energy basis and written as:

$$\hat{H}_A = \sum_{j=1}^{3} \hbar\omega_j |j\rangle \langle j| = \sum_{j=1}^{3} \hbar\omega_j \hat{\sigma}_{jj} \tag{2.2}$$

where $\hat{\sigma}_{ij} = |i\rangle \langle j|$ and is a *jump operator* for $i \neq j$ and a *projection operator* for $i = j$. The projection operators describe the atomic populations whilst jump operators describe the atomic coherences.

The Hamiltonian contribution due to the electric dipole interaction is given by $\hat{H}_{ED} = -e\hat{\mathbf{D}} \cdot \hat{\mathbf{E}}$ where $\hat{\mathbf{D}}$ is the dipole operator and $\hat{\mathbf{E}}$ is the electric field operator. Writing the dipole operator in terms of $\hat{\sigma}_{ij}$ operators yields:
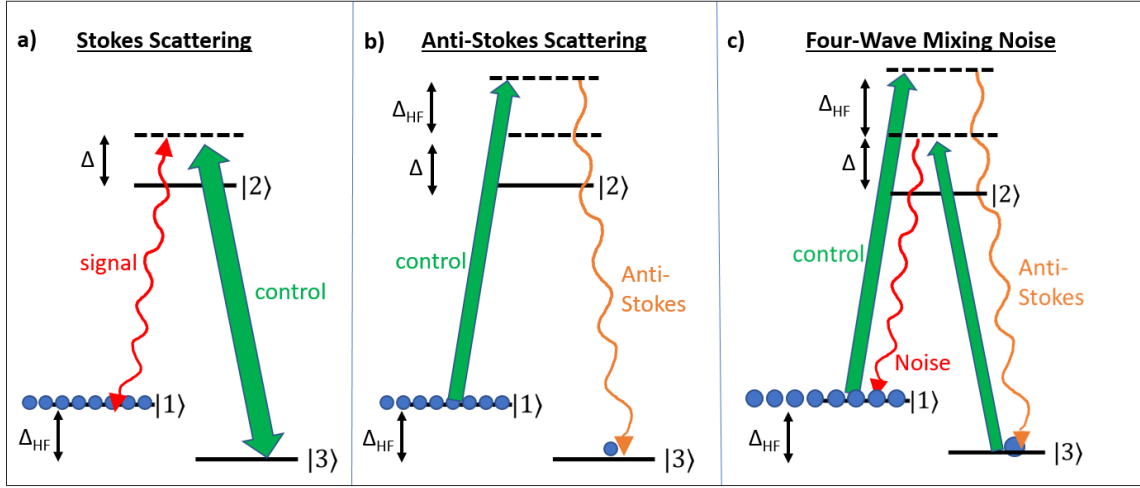
Figure 2.1: The Λ-level system used in the Raman memory protocol with the addition of the four-wave mixing noise. a) Shows the normal Stokes-Raman scattering used in the memory protocol. b) Shows the anti-Stokes photon (orange) produced by the control coupling to the populated level. c) Shows the four-wave mixing noise generated when the excitation produced by the anti-Stokes photon is read-out, producing noise (red) which are indistinguishable from signal photons.

$$\hat{\mathbf{D}} = \sum_{ij} \langle i| \hat{\mathbf{D}} |j\rangle \, \hat{\sigma}_{ij} = \sum_{ij} \mathbf{d}_{ij}\hat{\sigma}_{ij} \tag{2.3}$$

As the $|1\rangle \rightarrow |3\rangle$ transition is dipole forbidden $\mathbf{d}_{13} = 0$ and by the parity of the dipole operator (odd) $\mathbf{d}_{ii} = 0$. Equation 2.3 then becomes:

$$\hat{\mathbf{D}} = \mathbf{d}_{12}\hat{\sigma}_{12} + \mathbf{d}_{23}\hat{\sigma}_{23} + h.c. \tag{2.4}$$

2.1.1 Optical Fields

The free-field Hamiltonian describes excitations of the electromagnetic field and is given by:

$$\hat{H}_L = \int_0^\infty \mathrm{d}\omega \, \hbar\omega \hat{a}^\dagger(\omega)\hat{a}(\omega) \tag{2.5}$$

where the zero-point energy has been neglected and the photonic annihilation and creation operators $(\hat{a}(\omega), \hat{a}^\dagger(\omega))$ satisfy the bosonic commutation relation:

$$\left[\hat{a}(\omega), \hat{a}^\dagger(\omega')\right] = \delta(\omega - \omega') \tag{2.6}$$

For the three electric fields we may treat the bright control field classically but the signal and anti-stokes fields must be considered quantum mechanically, as ultimately we wish to model single-photon storage. If we consider the beams to have low divergence we can confine them to one-dimensional propagation. This yields the following equations for the electric fields:

$$\mathbf{E_c}(z,t) = \mathbf{v_c} E_c(z,t) e^{i\omega_c(t-z/c)} + c.c. \tag{2.7}$$

$$\mathbf{E_s}(z,t) = i\mathbf{v_s} \int d\omega\, g_s(\omega) \hat{a}_s(\omega,t) e^{-i\omega z/c} + h.c. \tag{2.8}$$

$$\mathbf{E_a}(z,t) = i\mathbf{v_a} \int d\omega\, g_a(\omega) \hat{a}_a(\omega,t) e^{-i\omega z/c} + h.c. \tag{2.9}$$

where the mode amplitude is given by $g(\omega) = \sqrt{\frac{\hbar\omega}{4\pi\epsilon_0 cA}}$ for a beam with area A. Assuming the bandwidth is small compared to the central frequency means the ω dependency of amplitude may be neglected and we can define $g_s = \sqrt{2\pi} g(\omega_s)$ (and similarly for g_a).

We may then write the three electric fields as:

$$\mathbf{E_c}(z,t) = \mathbf{v_c} E_c(z,t) e^{i\omega_c(t-z/c)} + c.c. \tag{2.10}$$

$$\mathbf{E_s}(z,t) = i\mathbf{v_s} g_s \hat{S}(z,t) e^{i\omega_s(t-z/c)} + h.c. \tag{2.11}$$

$$\mathbf{E_a}(z,t) = i\mathbf{v_a} g_a \hat{A}(z,t) e^{i\omega_a(t-z/c)} + h.c. \tag{2.12}$$

where the mode amplitudes are:

$$\hat{S}(z,t) = e^{-i\omega_s(t-z/c)} \times \frac{1}{\sqrt{2\pi}} \int d\omega\, \hat{a}_s(\omega) e^{-i\omega z/c} \tag{2.13}$$

$$\hat{A}(z,t) = e^{-i\omega_a(t-z/c)} \times \frac{1}{\sqrt{2\pi}} \int d\omega\, \hat{a}_a(\omega) e^{-i\omega z/c} \tag{2.14}$$

2.1.2 Time Evolution

The time evolution of the coherences is given by Heisenberg's equation of motion $\partial_t \hat{\sigma}_{ij} = i\left[\hat{\sigma}_{ij}, \hat{H}\right]$ and result in the following equations[23][27]:

$$\partial_t \hat{\sigma}_{11} = -i\hat{\mathbf{E}} \cdot (\mathbf{d_{12}}\hat{\sigma}_{12} + h.c.) \tag{2.15}$$

$$\partial_t \hat{\sigma}_{33} = +i\hat{\mathbf{E}} \cdot (\mathbf{d_{23}}\hat{\sigma}_{23} + h.c.) \tag{2.16}$$

$$\partial_t \hat{\sigma}_{12} = i\omega_{21}\hat{\sigma}_{12} - i\hat{\mathbf{E}} \cdot [\mathbf{d_{12}^*}(\hat{\sigma}_{11} - \hat{\sigma}_{22}) + \mathbf{d_{23}}\hat{\sigma}_{13}] \tag{2.17}$$

$$\partial_t \hat{\sigma}_{23} = i\omega_{32}\hat{\sigma}_{23} - i\hat{\mathbf{E}} \cdot [\mathbf{d_{23}^*}(\hat{\sigma}_{22} - \hat{\sigma}_{33}) - \mathbf{d_{12}}\hat{\sigma}_{13}] \tag{2.18}$$

$$\partial_t \hat{\sigma}_{13} = i\omega_{31}\hat{\sigma}_{13} - i\hat{\mathbf{E}} \cdot [\mathbf{d_{23}^*}\hat{\sigma}_{12} - \mathbf{d_{12}^*}\hat{\sigma}_{23}] \tag{2.19}$$

where $\omega_{ij} = \omega_i - \omega_j$ and by definition $\sum_{i=1}^3 \sigma_{ii} = 1$.

Throughout the derivation in Appendix A.1 the following assumptions are made:

1. The number of signal photons stored in the memory is much less than the total number of atoms meaning that $\partial_t \hat{\sigma}_{ii} = 0$. Higher order terms in signal $\hat{S}$, anti-Stokes field $\hat{A}$ and coherences σ_{ij} are neglected, since these are assumed to be small.

2. By transforming to a rotating frame and defining $\tilde{\sigma}_{ij} = \hat{\sigma}_{ij} e^{\omega_{ij}\tau}$ where τ is the retarded time $\tau = t - z/c$ we may neglect terms which oscillate much faster than the detunings. This is the rotating-wave approximation.

These approximations then yield the following equations for the interaction if imperfect pumping is assumed so the the proportion of atoms in the ground state is $(1 - \alpha)$:

$$\partial_t \tilde{\sigma}_{12} = -ie^{i\Delta_s\tau} \left[(1 - \alpha)\mathbf{d}_{12}^* \cdot (i\mathbf{v}_s g_s \hat{S} + \mathbf{v}_c E_c e^{i\omega_b\tau} + i\mathbf{v}_a g_a \hat{A} e^{2i\omega_b\tau}) \right.$$
$$\left. + \mathbf{d}_{23} \cdot \tilde{\sigma}_{13}(i\mathbf{v}_s g_s \hat{S} e^{-i\omega_b\tau} + \mathbf{v}_c E_c + i\mathbf{v}_a g_a \hat{A} e^{i\omega_b\tau}) \right] \tag{2.20}$$

$$\partial_t \tilde{\sigma}_{23} = -ie^{-i\Delta_a\tau} \left[\mathbf{d}_{12} \cdot \tilde{\sigma}_{13}(i\mathbf{v}_s^* g_s \hat{S}^\dagger e^{i\omega_b\tau} - \mathbf{v}_c^* E_c^* + i\mathbf{v}_a^* g_a \hat{A}^\dagger e^{-i\omega_b\tau}) \right.$$
$$\left. - \alpha \mathbf{d}_{23}^* \cdot \tilde{\sigma}_{13}(-i\mathbf{v}_s^* g_s \hat{S}^\dagger e^{2i\omega_b\tau} + \mathbf{v}_c^* E_c^* e^{i\omega_b\tau} - i\mathbf{v}_a^* g_a \hat{A}^\dagger) \right] \tag{2.21}$$

$$\partial_t \tilde{\sigma}_{13} = i \left[\mathbf{d}_{12}^* \cdot \tilde{\sigma}_{23} e^{i\Delta_a\tau}(i\mathbf{v}_s g_s \hat{S} e^{-i\omega_b\tau} + \mathbf{v}_c E_c + i\mathbf{v}_a g_a \hat{A} e^{i\omega_b\tau}) \right.$$
$$\left. - \mathbf{d}_{23}^* \cdot \tilde{\sigma}_{12} e^{-i\Delta_s\tau}(i\mathbf{v}_s^* g_s \hat{S}^\dagger e^{i\omega_b\tau} + \mathbf{v}_c^* E_c^* - i\mathbf{v}_a^* g_a \hat{A}^\dagger e^{-i\omega_b\tau}) \right] \tag{2.22}$$

From these equations it is hard to gain an intuitive picture of what is happening; it is useful therefore to consider these equations without the noise processes. To do this we assume the following (1) perfect pumping ($\alpha = 0$), (2) no anti-Stokes field ($\hat{A} = 0$) and (3) no undesired couplings ($\mathbf{d}_{12} \cdot \mathbf{v}_c = 0$). In this regime, with the previous assumptions, $\tilde{\sigma}_{23} \to 0$ the other two equations become:

$$\partial_t \tilde{\sigma}_{12} = \mathbf{d}_{12}^* \cdot \mathbf{v}_s g_s \hat{S} e^{i\Delta_s\tau} - i\mathbf{d}_{23} \cdot \mathbf{v}_c E_c e^{i\Delta_s\tau} \tilde{\sigma}_{13} \tag{2.23}$$

$$\partial_t \tilde{\sigma}_{13} = \mathbf{d}_{23} \cdot \mathbf{v}_c^* E_c^* e^{-i\Delta_s\tau} \tilde{\sigma}_{12} \tag{2.24}$$

Here the memory interaction becomes apparent. A signal field generates a coherence between $|1\rangle$ and $|2\rangle$. This - in the presence of a control field - couples to the ground state coherence $\tilde{\sigma}_{13}$ which takes the form of a spin-wave excitation defined below in equation 2.32. The signal is hence mapped coherently to (and hence stored in) the spin-wave.

2.1.3 Field Propagation

From Maxwell's equations it can be shown how the signal and anti-Stokes fields will propagate through the atomic ensemble. The atoms act like a dielectric medium and hence the fields propagate as:

$$\left[\nabla^2 - \frac{1}{c^2}\partial_t^2 \right] \hat{\mathbf{E}}_s = \mu_0 \partial_t^2 \hat{\mathbf{P}}_s \tag{2.25}$$

$$\left[\nabla^2 - \frac{1}{c^2}\partial_t^2 \right] \hat{\mathbf{E}}_a = \mu_0 \partial_t^2 \hat{\mathbf{R}}_a^\dagger \tag{2.26}$$

where $\hat{\mathbf{P}}_s$ and $\hat{R}_a^\dagger$ are the dipole moment per unit volume which oscillate at the field frequency. Atomic polarisations can therefore be written as $\tilde{\mathbf{P}}_s = \hat{\mathbf{P}}_s e^{-i\omega_s\tau}$ and $\tilde{\mathbf{R}}_a^\dagger = \hat{\mathbf{R}}_a^\dagger e^{-i\omega_a\tau}$ By making the paraxial approximation and assuming the amplitude of the envelope varies slowly we can write [23][27]:

$$\left(\frac{i}{2k_s}\nabla_\perp^2 + \partial_z + \frac{1}{c}\partial_t \right) \hat{S} = -\frac{\mu_0\omega_s^2}{2g_s k_s}\mathbf{v}_s^* \cdot \tilde{\mathbf{P}}_s \tag{2.27}$$

$$\left(\frac{i}{2k_a}\nabla_\perp^2 + \partial_z + \frac{1}{c}\partial_t \right) \hat{A} = -\frac{\mu_0\omega_a^2}{2g_a k_a}\mathbf{v}_a^* \cdot \tilde{\mathbf{R}}_a^\dagger \tag{2.28}$$

$$\tag{2.29}$$

where $k_{s,a} = \omega_{s,a}/c$.

Collective polarisation operators P and $R^\dagger$ and spin wave operator B may be defined by summing contributions to coherences σ_{ij} across the ensemble:

$$P = \frac{1}{\sqrt{n\delta V}} \sum_{\beta(\mathbf{r})} \tilde{\sigma}_{12}^\beta e^{-i\Delta_s\tau} \tag{2.30}$$

$$R^\dagger = \frac{1}{\sqrt{n\delta V}} \sum_{\beta(\mathbf{r})} \tilde{\sigma}_{23}^\beta e^{i\Delta_a\tau} \tag{2.31}$$

$$B = \frac{1}{\sqrt{n\delta V}} \sum_{\beta(\mathbf{r})} \tilde{\sigma}_{13}^\beta \tag{2.32}$$

where n is the number density and β labels all the atoms in a small volume δV at position $\mathbf{r}$. It can be shown that these satisfy the bosonic commutation relation as in equation 2.6. $P, R^\dagger$ and B can therefore be thought of as annihilation operators for atomic polarisations and spin-wave excitation.

Following the next steps of the derivation in A.2 we reach the final equations to describe the spin-wave (B) and the signal/anti-Stokes (S/A) fields:

$$(c\partial_z + \partial_t)\hat{S} = ic\sqrt{\frac{d\gamma_s}{L}}\frac{\Omega_{23}}{\Gamma_s}\hat{B} - \kappa_s\hat{S} \tag{2.33}$$

$$(c\partial_z + \partial_t)\hat{A} = ic\sqrt{\frac{d\gamma_a}{L}}\frac{\Omega_{12}}{\Gamma_a}\hat{B}^\dagger - \kappa_a\hat{A} \tag{2.34}$$

$$\partial_t\hat{B} = -i\Omega_{23}^*\sqrt{\frac{d\gamma_s}{L}}\left[\frac{(1-\alpha)}{\Gamma_s} + \frac{\alpha}{\Gamma_s^*}\right]\hat{S} + i\Omega_{12}^*\sqrt{\frac{d\gamma_a}{L}}\left[\frac{(1-\alpha)}{\Gamma_a} + \frac{\alpha}{\Gamma_a^*}\right]\hat{A}^\dagger$$
$$- \left[\frac{|\Omega_{12}|^2}{\Gamma_a^*} + \frac{|\Omega_{23}|^2}{\Gamma_s}\right]\hat{B} \tag{2.35}$$

Where $\kappa_s = \frac{d\gamma_s}{\tau}\left[\frac{(1-\alpha)}{\Gamma_s} + \frac{\alpha}{\Gamma_s^*+i\omega_b}\right]$, $\kappa_a = \frac{d\gamma_a}{\tau}\left[\frac{(1-\alpha)}{\Gamma_a+i\omega_b} - \frac{\alpha}{\Gamma_a^*}\right]$ with the complex detuning $\Gamma_{s,a} = \gamma_{s,a} + i\Delta_{s,a}$. These are in excellent agreement with the equations given in [52].

2.2 Green's Function Description

The linear nature of equations (2.33)-(2.35) means that a set of Green's functions $G_{jk}(z,\tau)$ describe the map between coherences and fields (for example the transformation spin-wave to signal field is described by G_{BS}). The spin-wave at the end of the read-in stage may hence be described as[7]:

$$B_{\text{out}}(z) = \int_{-\infty}^{\infty} G_{SB}(z,\tau)S_{\text{in}}(\tau)\mathrm{d}\tau + \int_{-\infty}^{\infty} G_{AB}(z,\tau)A_{\text{vac}}^\dagger(\tau)\mathrm{d}\tau + \int_{-\infty}^{\infty} G_{BB}(z,z')B_{\text{therm}}(z')\mathrm{d}z' \tag{2.36}$$

where "vac" and "therm" denote initial vacuum and thermal states for the anti-Stokes and spin-wave fields respectively. A similar expression can hence describe the retrieved signal field:

$$S_{\text{out}}(\tau) = \int_{-\infty}^{\infty} G_{BS}(z,\tau)B_{\text{out}}(z)\mathrm{d}z + \int_{-\infty}^{\infty} G_{AS}(\tau,\tau')A_{\text{vac}}^{\dagger}(\tau')\mathrm{d}\tau' + \int_{-\infty}^{\infty} G_{SS}(\tau,\tau')S_{\text{vac}}(\tau')\mathrm{d}\tau'$$
$$(2.37)$$

The expectation values $N_x = \langle \int_{-\infty}^{\infty} S_x^{\dagger}(\tau)S_x(\tau)\mathrm{d}\tau \rangle$ gives the number of input and output signal photons for $x = \text{in/out}$. The total efficiency is normally defined as $\eta_{\text{tot}} = N_{\text{out}}/N_{\text{in}}$ however the noise from four-wave mixing provides a means for this efficiency to be greater than 1. Nunn et al. [52] use a modified definition for total efficiency where they subtract the spontaneous signal photons outputted with no input signal:

$$\eta_{\text{tot}} = \frac{\tilde{N}_{\text{out}}}{N_{\text{in}}} \qquad \tilde{N}_{\text{out}} = N_{\text{out}} - N_{\text{out}|\text{no input}} \qquad (2.38)$$

With a full numerical simulation this provides a means for calculating efficiency, and analysis of the Green's functions provides a measure of noise.

2.3 Noise Suppression

Four-wave mixing has been identified as the key contributor to noise in these systems[7] and as a result numerous efforts have been made to reduce this noise. The noise caused by four-wave mixing (number of photons emitted during the readout pulse without an input signal) has been measured at 0.15±0.05 photons per pulse[23]. This is, however, still too high for single photon storage. This section will describe two recent proposals to suppress this noise floor: the first is a recently demonstrated suppression method using a cavity and in the second the detuning is chosen such that the anti-Stokes field is strongly absorbed. Simulation and analysis of the second method will be discussed in the following section.

2.3.1 Cavity

A recent demonstration of noise suppression by Saunders et al.[53] showed the noise floor lowered to $(15\pm2)\times 10^{-3}$ photons per pulse by placing the atomic ensemble in a low-finesse birefringent cavity. The birefringent element allowed both the signal and the orthogonally polarised control fields to exist in cavity modes whilst simultaneously being anti-resonant with the anti-Stokes field as shown in Figure 2.2.
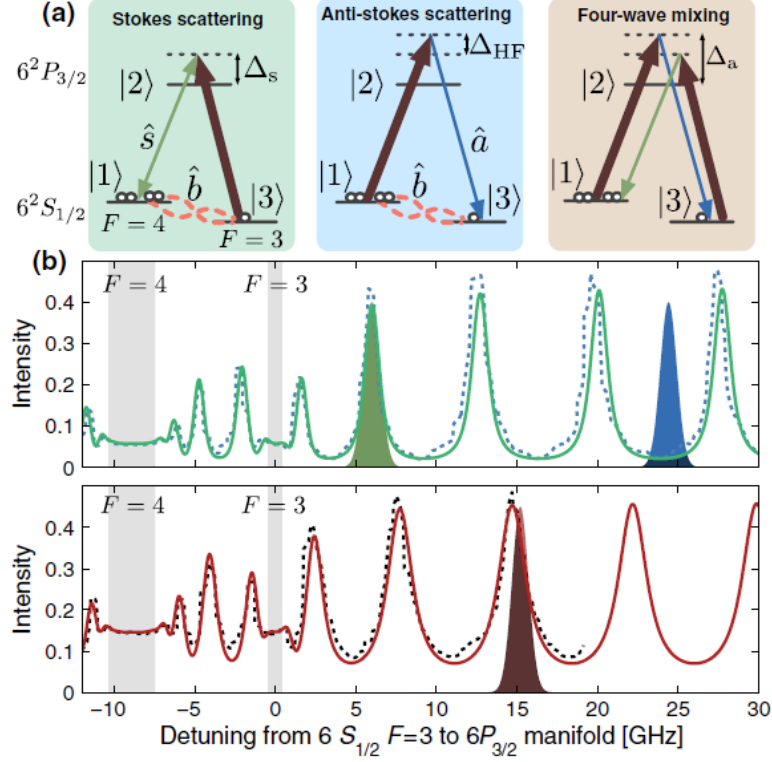
Figure 2.2: a) The energy level structure used in the cavity enhanced Raman memory showing the interactions of the signal (green), control (red) and anti-Stokes (blue) that produces four-wave mixing noise. b) The cavity modes used in the enhanced memory showing that the signal and cavity frequencies are supported whilst the anti-Stokes frequency is anti-resonant. The dashed lines are the measured responses of the cavity whilst the solid are the estimated response. Figure from [53].

The enhancement this system results in are twofold. Firstly, the cavity reduces the density of states at the anti-Stokes frequency and secondly the cavity acts to enhance the Raman coupling, reducing the control power required. The results of this experiment will be discussed further in Section 3.1.

2.3.2 Absorption

In 2016 Romanov et al. presented a proposal to reduce the effect of four-wave mixing in a three level system by engineering a Raman absorption feature on resonance with the noise field[54] as shown in Figure 2.3. They showed theoretically that suppressing the four-wave mixing noise did not affect the coherence created in their EIT memory scheme. They tested the proposal making use of the two naturally occuring isotopes of Rubidium with ^{87}Rb used to implement EIT and ^{85}Rb for the absorption, which have abundances 72% and 28% respectively. Experimentally they demonstrated the success of this method to suppress four-wave mixing but their implementation of EIT suffered as a result of their probe being absorbed in the wings of ^{85}Rb resonance.
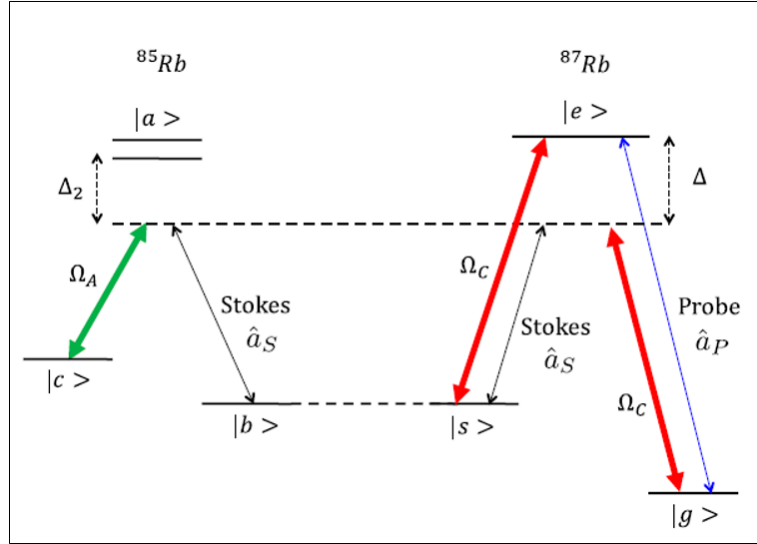
Figure 2.3: Energy level diagram for the two isotopes of Rb used. The EIT memory protocol is shown in ^{87}Rb with the on-resonance probe $\hat{a}_P$ (blue) and control Ω_C (red). The four-wave mixing is due to the Raman scattering caused by the control coupling to the ground $|g\rangle$ producing a Stokes photon $\hat{a}_S$ (black) resulting in an unwanted coherence between the ground and storage state $|s\rangle$. By applying a second (Raman) control field Ω_A (green) the Stokes field is absorbed in the induced Raman absorption resonance in the ^{85}Rb. Figure from [54]

This principle of absorbing the four-wave mixing noise can hopefully be applied to the Raman memory protocol in caesium which we are currently developing in Oxford. With only one stable isotope of caesium the same scheme cannot be carried over exactly. Instead the detuning is arranged such that the anti-Stokes field is on-resonance with the populated transition as shown in Figure 2.4.

In this configuration we expect the four-wave contribution to be significantly reduced. There are, however, potential disadvantages to this approach, which will require future theoretical and experimental investigation. The two primary areas in which this configuration may suffer is firstly the control field detuning from the populated transition is decreased, which could increase the effect of the AC-Stark shift induced by the strong control field. The result of this is reduced efficiency due to the change of energy level. Furthermore the signal detuning is also increased which reduces the coupling strength of the Raman interaction $\left(C_s \propto \sqrt{N}\left(\frac{\Omega_c}{\Delta}\right)\right)$ meaning the control field might need to be increased to compensate (further increasing the AC-Stark effect). A stronger control field is also requried as the control field suffers from higher linear absorption the less detuned it is from the populated transition as can be seen in Figure 2.4.

In the next two sections, I'll present simulation results of this detuning configuration and suggest further developments for the model.
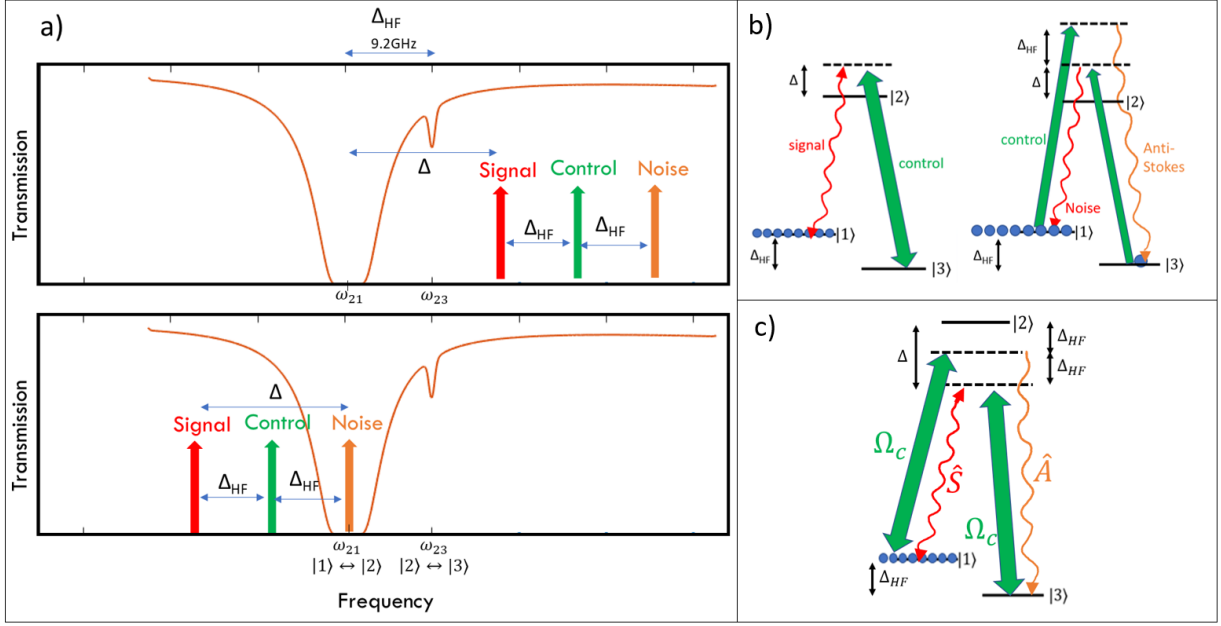
Figure 2.4: a) The transmission function for Caesium pumped into the ground state $|1\rangle$ with the frequencies of the three fields used for (top) the usual Raman protocol and (bottom) the absorption method shown. The small dip at ω_{23} is due to imperfect pumping. b) Left shows the memory transition in normal Raman, Right shows the noise process where noise is added to the signal frequency c) The energy level and detuning structure used for the absorbative noise suppression proposal with the fields shown. The detuning condition $\Delta = -2\Delta_{HF}$ can be clearly seen.

2.4 Simulation Results

To simulate the system we begin with a simplified version of the fully derived equations 2.33-2.35 where we assume 100% pumping efficiency ($\alpha = 0$) and that neither the control field's Rabi frequency nor the homogeneous line-width is transition dependent ($\Omega_{12} = \Omega_{23} = \Omega$ and $\gamma_s = \gamma_a = \gamma$). These equations are the same as those stated in [52] and are:

$$(c\partial_z + \partial_t)\hat{S} = ic\sqrt{\frac{d\gamma}{L}}\frac{\Omega}{\Gamma_s}\hat{B} - \kappa_s\hat{S}$$

$$(c\partial_z + \partial_t)\hat{A} = ic\sqrt{\frac{d\gamma}{L}}\frac{\Omega}{\Gamma_a}\hat{B}^\dagger - \kappa_a\hat{A} \qquad (2.39)$$

$$\partial_t\hat{B} = -i\sqrt{\frac{d\gamma}{L}}\frac{\Omega^*}{\Gamma_s}\hat{S} + i\sqrt{\frac{d\gamma}{L}}\frac{\Omega^*}{\Gamma_a}\hat{A}^\dagger - \left[\frac{1}{\Gamma_s} + \frac{1}{\Gamma_a^*}\right]|\Omega|^2\hat{B}$$

where $\kappa_s = \frac{d\gamma}{\tau\Gamma_s}$ and $\kappa_a = \frac{d\gamma}{\tau(\Gamma_a + i\omega_b)}$ with the complex detuning $\Gamma_{s,a} = \gamma_{s,a} + i\Delta_{s,a}$ as before.

This system of equations cannot be solved analytically and hence must be solved numerically. To do this a combination of the Runge-Kutta method[55] and Chebyshev iteration method[56] is used with the method as follows:

1. A mesh in (z, t) space is chosen size ($N_z \times N_t$), with z spanning the length of the cell containing Caesium atoms and for the purpose of the simulation t goes from $0-8$ nanoseconds with read-in and read-out occurring at 2ns and 4ns respectively.

2. A matrix ρ combining S, A, B is initialised for $t = 0$ over all z (so the size of ρ is ($3 \times N_z$))

3. A function f is created such that $\dot{\rho} = f(t, \rho)$ where the Chebyshev method is used to generate the ∂_z differential of S and A implicit in $\dot{\rho}$.

4. Discretising ρ and t into time-steps ρ_n and t_s for n=$\{0, N_t\}$ we can define:

$$\rho_{n+1} = \rho_n + \frac{dt}{6}(k_1 + 2k_2 + 2k_3 + k_4) \quad \text{and} \quad t_{n+1} = t_n + dt$$

where (from the Runge-Kutta method):

$$k_1 = f(t_n, \rho_n) \qquad \qquad \text{The increment based on Euler's method.}$$

$$k_2 = f(t_n + \frac{dt}{2}, \rho_n + k_1\frac{dt}{2}) \quad \text{The increment based on } k_1 \text{ and the midpoint gradient.}$$

$$k_3 = f(t_n + \frac{dt}{2}, \rho_n + k_2\frac{dt}{2}) \quad \text{The increment based on } k_2 \text{ and the midpoint gradient.}$$

$$k_4 = f(t_n + dt, \rho_n + k_3 dt) \qquad \text{The increment based on } k_3 \text{ and the final gradient.}$$

5. The final output of this is a $(3 \times N_z \times N_t)$ tensor spanning all of (z, t) space for the 3 variables S, A, B.

To solve any differential equation we must also include both initial and boundary conditions. These conditions are quite simple. For spin-wave (B) and the anti-Stokes field (A) these are initialised to $B(t=0) = A(t=0, z) = 0$ for all z. For the signal field $S(t=0, z)$ we initialise with the tail of the Gaussian that will form our read-in signal peaking at $t = 2$ns. The boundary conditions follow from defining $z = 0$, and again for the spin-wave and anti-Stokes field these are initialised to zero. The signal's $z = 0$ boundary is defined simply by a Gaussian peaking at 2ns which forms the read-in signal. To simulate the control pulse being turned on $\Omega(t)$ is the sum of 2 Gaussians with peaks at 2ns (read-in) and 4ns (read-out).

For the majority of simulations the following parameters based on experimental values were used (unless otherwise stated):

Variable	Value
Optical depth (d)	1000
Line-width (γ)	6MHz
Rabi Frequency (Ω_{max})	5GHz
Interation Length (L)	0.072m
Pulse FWHM	300ps

Before investigating how noise changed as a function of detuning from the absorption condition $(\Delta = -2\Delta_{HF})$ I first had to check that the simulation was functioning realistically, and met the following criteria:

1. The presence of the control field causes signal to be absorbed and re-emitted at read-out.

2. Without the anti-Stokes noise presence, neither read-in nor read-out efficiency could be greater than 100%.

3. Total efficiency of the memory is calculated to be proportional to $1/\Delta^4$

With these three tests completed [Figure 2.5 a)-c)] I then looked at quantifying the noise caused by the anti-Stokes. As can be seen from Figure 2.4 the effect of the four-wave mixing is to add

27

intensity during the readout. This is exactly what Figure 2.5 (d) shows; there is more retrieved signal when the FWM interaction is included in the simulation. The metric used to quantify this noise is the following:

$$\text{Noise} = \int dt \frac{|Signal|^2_{AS} - |Signal|^2_S}{\int dt |Signal|^2_{AS}} \tag{2.40}$$

where $|Signal|^2_{AS/S}$ is the retrieved signal intensity with/without the anti-Stokes interaction and the integral is taken during the read-out. That is to say the noise metric could be thought of as the proportion of energy added by the anti-Stokes to the read-out signal.
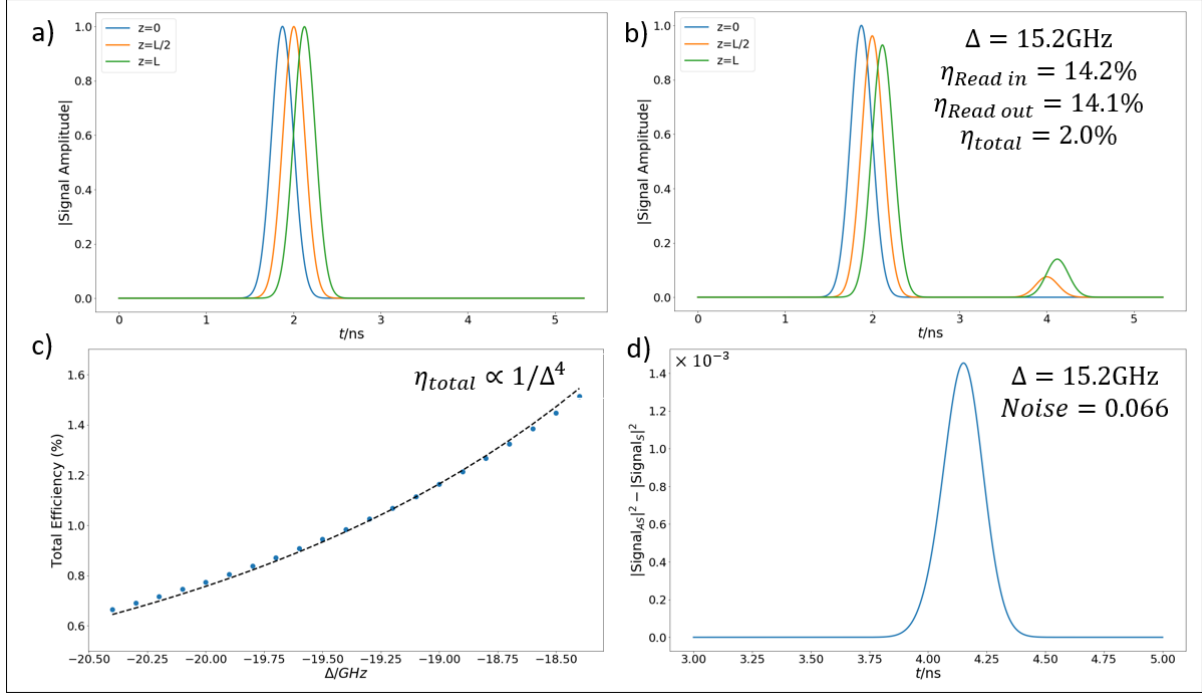

Figure 2.5: a) and b) The signal magnitude at the start, middle and end of the cell shown in blue, orange and green respectively. a) is simulated without the control field whilst b) is with. c) The efficiency as a function of detuning, blue shows simulated data points, black shows the agreement with the model $\eta_{total} \propto 1/\Delta^4$. d) The difference in the signal field's intensity at read-out with and without the anti-Stokes interaction. From the difference we are able to calculate a value for the noise, given by equation 2.40

The model is therefore shown to agree with prediction, and to act physically. To quantify the noise suppression of the proposed absorption method I simulated the memory at a range of detunings around the detuning condition $\Delta = -2\Delta_{HF} = -18.4\text{GHz}$. This was successful and showed a noise suppression at this condition by a factor of over five orders of magnitude compared to the memory's normal detuning $\Delta = 15.2\text{GHz}$ (Figure 2.6). The simulation is however shown to to suffer from numerical instabilities; these can be seen when the detuning from the absorption condition is sampled more frequently [Figure 2.6 b)].
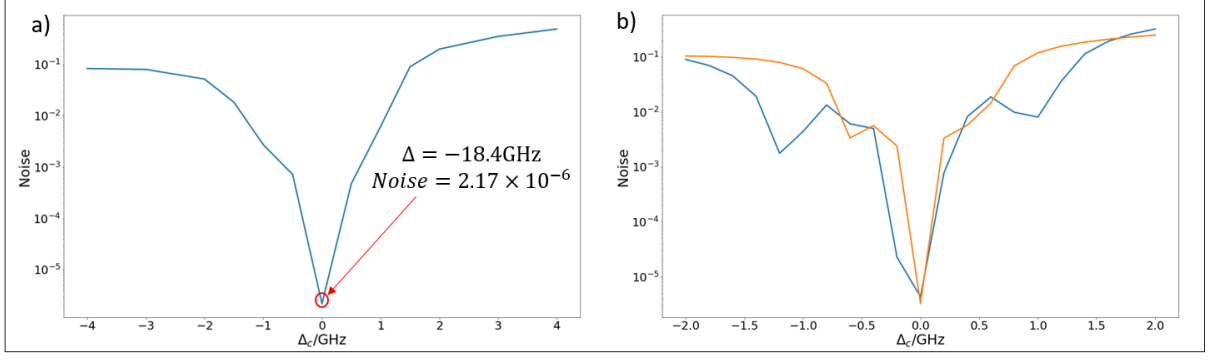
Figure 2.6: Noise as a function of detuning from the absorption condition ($\Delta_c = \Delta + 18.4$GHz). a) Shows a larger frequency range whilst b) blue shows numerical instabilities as detuning is sampled more frequently. The orange line shows the effect of increasing N_z by a factor of 2 and N_t by a factor of 4 which is shown to stabilise the numerics.

2.5 Conclusion

In conclusion, the equations of motion for the Raman memory protocol have been derived which include the contribution caused by four-wave mixing. These equations were then simulated to test a proposed absorbative noise suppression scheme. The simulation supported the proposal with noise dropping from 0.066 to 2.17×10^{-6}; a suppression factor of over 3×10^{-5}.

The numerical solving of the differential equations was shown to suffer from instabilities which could be addressed by increasing the precision of the simulation at the cost of solving time. Additionally, due to the nature of the equations, an increase in the precision of z by a factor α means the precession of t must increase by a factor of α^2. For this reason both the possibility of running the simulation on a computing cluster and using an alternative solving method are being investigated.

Future development of this simulation will see the Green's functions described in equations 2.36-2.37 simulated which will allow a more quantitative measure of noise. It will also allow the four-wave mixing to be modelled as the result of vacuum fluctuations whereas the current simulation requires it to be seeded by an input signal.

Chapter 3

Experiment

The Raman memory experiment with the Ultra-fast Quantum Optics (UFQO) at the University of Oxford has been developing and growing over the last decade. The result of such a undertaking is an intricate and complex arrangement of electronics and optics which require up to months of tutelage in order to use and to use safely. My project was therefore split following two research strands 1) Investigating the Raman memory's equations of motion and simulating the absorptive noise suppression scheme numerically presented in the previous chapter and 2) being trained on the experimental apparatus and working towards implementing an experimental test of the proposed suppression method. The experimental pursuit was hindered by the principle laser used requiring maintenance during the early part of my project.

This chapter will discuss the previous results of suppressing noise in the Raman memory before going on to discuss the experimental arrangement used to investigate the noise suppression scheme discussed in Section 2.3 and document the difficulties associated in realising it.

3.1 Overview of Previous Results

The possibility of the absorptive noise suppression scheme reducing the four-wave mixing noise (heavily supported by the results in Chapter 2) there is a real possibility of being able to store single-photons with the discussed experimental design. This would be a significant achievement and represent an important stepping stone in the realisation of a room-temperature broadband quantum memory. This section will just outline the significant development of the implementation of the Raman memory since its conception in 2007[5][35].

- (2010) The Raman memory was first demonstrated with a coherent state demonstrating storage time of 12.5 ns and a total efficiency of 15%. The coherence of the retrieved pulse is demonstrated by the observation of interference fringes between the retrieved state and a delayed copy of the input state. The maximum fringe visibility of $86 \pm 5\%$ supported the demonstrated that memory interaction is coherent [36].

- (2011) Weak coherent light, $\langle n \rangle = 1.6$, was stored for 4 μs with total efficiency of 15%. An unconditional noise floor of 0.25 photons per pulse was observed and attributed to four-wave mixing [43].

- (2012) The ability to store polarisation encoded information is demonstrated to be able to be stored in the memory using a *dual-rail* architecture. Horizontal and vertical polarisations are split into two beam-paths through the memory before being recombined

after the memory, in this way and arbitrary polarisation can be stored. This was demonstrated with 97% fidelity, dropping to 86% for a 1.5 μs storage time, this was despite no improvement in efficiency (30%) storing $\langle n \rangle = 10^4 - 10^5$[57].

- (2016) A cavity was used to suppress four wave mixing in the way described in Section 2.3.1 with the noise floor lowered to $(15 \pm 2)10^{-3}$ photons per pulse and a total efficiency of $(9.5 \pm 0.5)\%$ for the storage of weak coherent states with $\langle n \rangle = 0.7$.

It is useful at this point to define a metric for noise given by:

$$\mu_1 = \frac{\langle n^{noise} \rangle}{\eta_{total}} \tag{3.1}$$

since this combines the average number of noise photons produced $\langle n^{noise} \rangle$ and total efficiency. In the case of single photon storage this could be thought of as the relative probability of the retrieved photon having come from noise given a photon was sent into the memory. That is to say with a $\mu_1 = 1$ if a single photon is sent into the memory, it is equally likely that the retrivied photon comes from noise as it is the signal. It may be approximately related to fidelity by $\mathcal{F} \approx 1 - \mu_1$ and hence for maintaining quantum statistics mu_1 should be ≤ 0.01. The cavity saw the μ_1 reduce by a factor of 3 from ≈ 0.5 to ≈ 0.17. It is hoped that the absorbative noise suppression method can reduce this further.

3.2 Experimental Arrangement

This section will describe the key components of the experimental infrastructure including the preparation of the signal/control fields, the storage medium and the detection apparatus and procedure.

3.2.1 Caesium

The Λ-system used in our implementation of the Raman memory protocol is an ensemble of atomic caesium vapour with the D_2 line at 852 nm. The hyperfine splitting in the $6S_{1/2}$ ground-states ($F = 3, 4$) provide the levels $|1\rangle$ and $|3\rangle$ for the memory with a splitting of 9.2 GHz[1]. The upper state $6P_{3/2}$ is actually a manifold of hyperfine levels ($F = 2, 3, 4, 5$) each separated by an average splitting of $\approx$ 200MHz however addressing these levels individually is not possible at room temperature due to Doppler broadening[23] so they are treated as a single state. For the memory to be implemented two conditions must be satisfied; firstly the control and signal frequencies must be separated by 9.2 GHz to satisfy the two-photon Raman scattering condition and secondly, the system must be initialised to the $|1\rangle$ state, achieved by pumping the $|2\rangle \leftrightarrow |3\rangle$ transition before the signal is sent into the memory. The relevant atomic energy levels are shown in Figure 3.1.

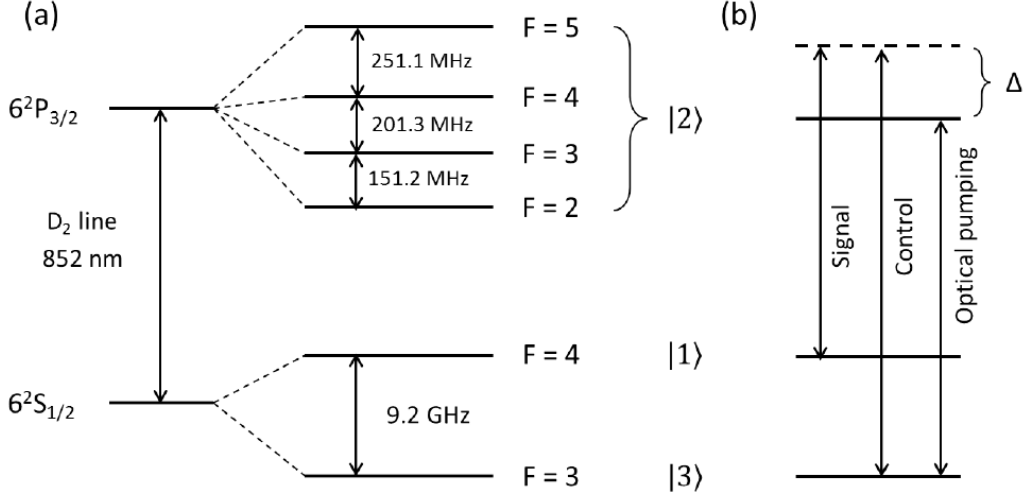[1]These are the famous clock states used to define the second[58].

Figure 3.1: (a) Atomic structure of caesium showing the splitting between energy levels (b) Λ-system with the signal, control and optical pumping frequencies shown in the caesium energy structure (figure not to scale).

The caesium vapour is contained in a cylindrical glass cell with anti-reflection coated windows so that it may be addressed optically. Recalling that the Raman coupling strength is proportional to $\sqrt{N}$ (equation 1.3) it is beneficial to increase the number density, which is related to vapour pressure and temperature by the ideal gas law: $n(T) = P_v(T)V/RT$. Vapour pressure is shown to exponentially increase with temperature[27], and hence heating the cell will increase the number-density (and therefore the coupling). The benefit from heating is found to saturate at approximately $70\,^{\circ}\mathrm{C}$ due to the process of *radiation trapping*[59] which results in imperfect pumping as a result of spontaneously emitted photons being re-absorbed.

A buffer gas is also added to the vapour cell to inhibit diffusion of the atoms from the beam's path within the cell. A buffer gas must have spin-preserving collisions with the caesium atoms so not to cause decoherence and shorten the memory's lifetime and efficiency. Spin-flip decoherence can also occur by collision with the cell wall by collisions with other caesium atoms. The decoherence from the cell walls can possibly be increased with a spin-preserving chemical coating whilst the caesium-caesium collisions can are shown to restrict the coherence time to tens of milliseconds[60].

Finally, the Earth's magnetic field can also cause the spin-wave to experience decoherence due to dephasing of Zeeman split sub-levels. This effect can be reduced in two ways: the first is a passive means where the vapour is shielded by a μ-metal which has a permeability, the second is an active method where a collection of Helmholtz coils are placed around the sample to create a constant magnetic field that cancels exactly with the Earth's field[61]. Currently the first method is employed but I am currently investigating the feasibility of an active method.

3.2.2 Signal and Control Fields

The principle laser used in the experiment is a mode-locked titanium-sapphire (Ti:Sa) laser with a repetition rate of $80\,\mathrm{MHz}$ producing pulses of approximately $360\,\mathrm{ps}$ and a transform limited bandwidth of $1.2\,\mathrm{GHz}$. The Ti:Sa laser has the ability to be tuned and locked to a frequency over a range of tens of GHz surrounding 852nm, achieved by an active PID lock and is stable to $\sim 100\,\mathrm{MHz}$[23]. The detuning condition for the absorbative noise suppression scheme is that the signal detuning be $\Delta = -2\Delta_{HF} = -18.4\,\mathrm{GHz}$ from the $|1\rangle \leftrightarrow |2\rangle$ transition (as shown in

Figure 2.4). The control detuning is therefore $-9.2\,\text{GHz}$ and it is this frequency that the Ti:Sa laser will be locked to since we need significantly more power in the control pulse.

To generate the signal frequency the Ti:Sa beam is sent through a polarising beam-splitter at the start of what is a unbalanced (in intensity) Mach-Zender interferometer. The weaker arm forms the basis of the signal and is sent through an eletro-optic modulator (EOM) driven by a 9.2 GHz radio-frequency (RF) amplifier. This generates side bands 9.2 GHz red- and blue-detuned sidebands from the control (carrier) frequency. The signal we want to use for the signal is the red-detuned output and so the carrier and blue-detuned sideband are filtered with a Fabry-Perot etalon.

The signal (now at the correct frequency) is then recombined with the strong control beam at a beam-splitter before being sent into the memory. A delay in the control field beam-path is in place to allow maximum overlap with the signal. At a later time another control pulse will be sent for the read-out. This timing is achieved by a combination of the Pockels cell which has the ability to selectively pick pulses from the 80 MHz Ti:Sa repetition rate, and by the EOM which is only turned on during the read-in signal - this ensures no signal is sent to the memory during the read-out procedure. The optical pumping is turned of for the memory operation so not to destroy the stored spin-wave coherence. Following the read-out control pulse, the retrieved signal is then filtered from the so the signal can be sent to detectors. The experimental set-up described here is shown in Figure 3.2.
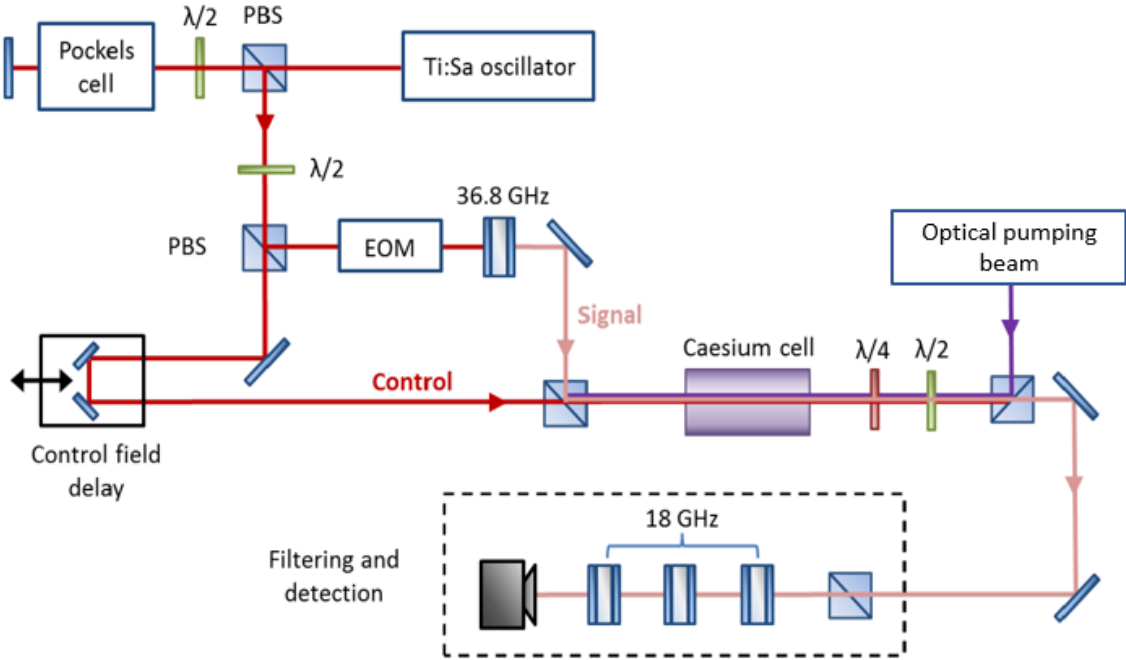

Figure 3.2: Experimental set-up to test the absorbative noise suppression scheme in the Raman memory. The Pockels cell selectively picks pulses from the titanium-sapphire (Ti:Sa) laser to send to the memory which are then separated by a polarising beam-splitter (PBS). The signal frequency is generated as one of two side-bands produced by an eletro-optic modulator (EOM) which has the other sideband and carrier pulse filtered by a Fabry-Perot etalon with free spectral range (FSR) = 36.8 GHz. The signal and control pulses are then recombined before being focused into the memory (caesium cell). After a following control only pulse, the retrieved signal and control fields are separated by a polarising beam splitter and 3 Fabry-Perot etalons with FSR=18 GHz. The optical pump beam from another laser is shown counter-propagating to the signal and the control and is active only in the preparation stage of the memory. Figure adapted from [23].

3.2.3 Limiting Factors, Noise Processes and Solutions

The limiting factor in the experimental test of the noise suppression scheme comes from the technical noise from to the bright control pulse and separating this from the signal. Currently control power used in the normal operation of the memory is $\approx 1.4\,\text{nJ}$ which corresponds to $\approx 6 \times 10^9$ photons. To then separate these from a (in principle) single retrieved photon requires about 12 orders of magnitude suppression of the control. This can be achieved by polarisation frequency, and spatial filtering.

The polarisation and frequency filtering can be seen in Figure 3.2 by the polarising beam splitter and set of Fabry-Perot etalons with FSR=18 GHz (since the control and signal are separated by 9.2 GHz this places the control at the minimum of the etalon's transmission function). An extra etalon with FSR = 103 GHz has been added to further increase suppression. Spatial filtering involves coupling the signal mode though a single-mode fibre to help separate the signal from the control. These processes combined should be able to reach the required level of noise suppression.

Conclusion

This chapter has provided an overview of the significant milestones that the Raman memory has accomplished over the previous ten years, and discussed the experimental arrangement to investigate the proposed noise suppression. Investigation of this scheme is by no means simple with many possible experimental challenges but in parallel with the development of the theory as the noise processes are better understood I am confident that investigation of this avenue of research will benefit the understanding of the memory and progress the field towards a quantum memory for temporal multiplexing.

Chapter 4

Outlook

In this section I will outline three experiments that form logical avenues of the investigation should the Raman memory succeed in storing single photons with the noise suppression scheme discussed in this thesis.

4.1 Future Experiments

4.1.1 Photon Synchronization

As discussed in 1.2.1 the synchronization and multiplexing of heralded photons is a driving factor in the realisation of a quantum memory. Moreover the properties exhibited by the Raman memory (large storage bandwidth and microsecond lifetime) mean that it would produce a sufficiently high time-bandwidth product to yield enhanced multi-photon coincidence rates. The proof-of-principle demonstration could be achieved by interfacing the memory with a SPDC source[1] and storing a heralded single photon. Following the detection of a second herald photon the stored excitation in the memory is retrieved and its output synchronised with the photon that was emitted from the source. The rate of two-photon synchronisation from two sources ($\approx p^2 R$) where p is the probability of production and R is the repition rate of pump pulses) can be compared to the rate obtained by memory multiplexing ($\approx \frac{p}{(1-p)^2}\eta R/2$ where η is the memory efficiency). This could then be scaled up and demonstrated with a greater number of memories yielding larger multi-photon coincidences.

4.1.2 Light-matter Hong-Ou-Mandel effect

If two identical photons are incident on ports of a 50:50 beam-splitter they will exhibit the Hong-Ou-Mandel (HOM) effect[11] which is to say they will always exit from the same (but random) output port i.e. $|1\rangle |1\rangle \xrightarrow{Beam-splitter} \frac{1}{\sqrt{2}}(|2\rangle |0\rangle + |0\rangle |2\rangle)$ where the two photon Fock state is converted to a two-photon NOON-state. This can be used as a measure of photon indistinguishably[62] since the probability of the $|1\rangle |1\rangle$ state being detected after the beam-splitter is $1 - \text{Tr}(\rho_a \rho_b)$ where $\rho_{a,b}$ are the density matrices of the two emitted photons. It can therefore be used with an interferometer to accurately measure properties such as temporal waveforms[63].

Since the Raman memory can be described with the beam-splitter Hamiltonian (equation 1.3

---

[1]Spontaneous parametric down-conversion sources are discussed in Section 1.2.1

and Figure 4.1) the HOM effect should be able to be observed with optical and spin-wave modes in the following way:

1. The read-in and read-out efficiencies of the memory are tuned to 50% and a signal photon is sent to the memory (with a control pulse).

2. Conditional on the photon being stored (rather than transmitted) a a second single photon is input into the memory, again with a control pulse. Hence prior to the beam splitter operation the modes are $|B_{in}S_{in}\rangle$ where B and S represent spin-wave and signal modes. Here the possible outcomes of the beam-splitter interaction are that a) the second photon is stored resulting in two spin-wave modes stored in the memory and b) the second photon is transmitted *and* the stored photon is retrieved - two signal modes leave the memory. Hence the NOON-state $\frac{1}{\sqrt{2}}(|S_1 S_2\rangle + |B_1 B_2\rangle)$ is created.

3. A third read-out control pulse in applied to the memory, reading out a signal if a excitation was stored. The coincidence of a signal being detected in the 1st *and* 2nd of the read-out events should be zero if the input photons were identical.

This experiment would confirm the quantum nature of the Raman memory and provide an interesting way to probe the underlying physics of the spin-wave since the indistinguishability condition can be understood as identical photons generating identical spin-waves.
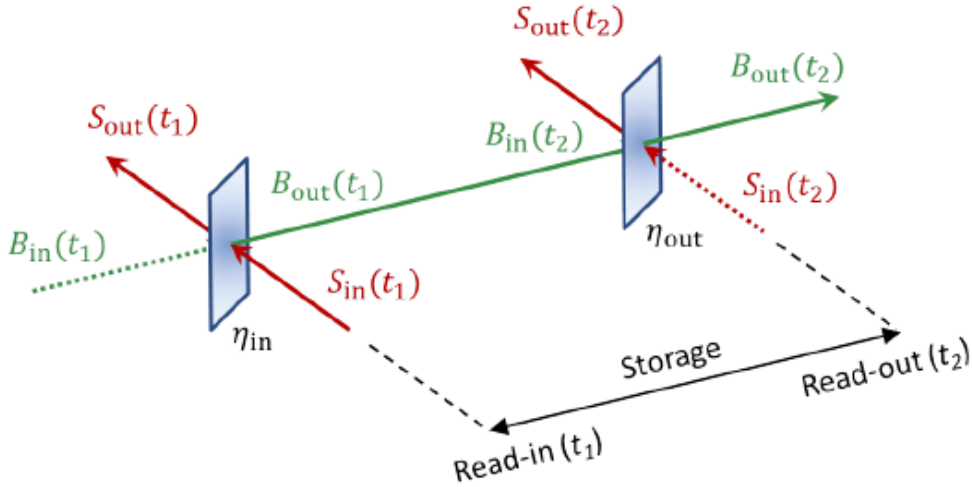

Figure 4.1: The Raman memory interaction as a beam splitter for optical $S_{in/out}$ and spin-wave modes $B_{in/out}$. Under normal operation the green and red dotted lines signify vacuum states, however during the HOM experiment $S_{in}(t_2)$ would be a photon to produce the state $\frac{1}{\sqrt{2}}(|S_1 S_2\rangle + |B_1 B_2\rangle)$

.

4.1.3 Temporal Modes Storage

In addition, the Raman memory has recently been demonstrated as being able to store a user-chosen temporal mode that is, a temporal pulse shape of a single photon. Temporal modes have been identified as promising basis states for quantum information processing[64]. The memory operated in this way could function the same way as a polarising beam splitter does for a polarisation encoding in QIP.

Furthermore the memory provides a simple temporal mode encoding to temporal mode and time-bin encoding: consider the memory storing the temporal mode basis state $|0\rangle$ and transmitting $|1\rangle$. An arbitrary state $\alpha|0\rangle + \beta|1\rangle$ is sent into the memory, and the memory is then read-out at a time dt later. The result is a double encoding $\alpha|00\rangle + \beta|11\rangle$, one in temporal modes, and one in the time domain. This property of the memory offers many exciting developments within QIP.

Conclusion

The need for a quantum memory is apparent in emerging quantum technologies and has grown into an incredibly active research area. A photonic quantum memory is quickly becoming a constituent part of many proposed architectures in quantum information processing with varying applications. The two primary applications explored are a quantum repeater and for temporal multiplexing but additional applications such as a temporal mode beam splitter are also being explored.

The requirements of these memories varies dependent on the application and can be quantified by a number of parameters including efficiency, signal to noise ration (SNR) and time-bandwidth product B, and lifetime to name a few. The variations in these figures of merit are equally matched by the variation in implementations which vary by both the protocol and storage media.

Chapter 1 provided a comprehensive review of the primary protocols used and discussed the state of the art comparing the leading experimental achievements in the field. The need for a large time-bandwidth product was identified as a key figure of merit in temporal multiplexing applications, illustrated by the example given for photon-synchronisation.

The Raman memory currently has all the components required for a broadband room temperature quantum memory except it suffers from prohibitive four-wave mixing noise preventing it from faithfully storing single photons. To analyse this noise process, Chapter 2 details the derivation and simulation of the Raman memory implemented with warm caesium vapour. The model is then used to explore a noise-suppression proposal and demonstrated the possibility for a significant reduction in noise (five orders of magnitude) with the proposed suppression scheme. The next step is to validate and support these theoretical results which is currently being investigated with the experimental set-up described in Chapter 3 where we also discussed results achieved by previous implementations of the Raman memory.Finally future experiments for the Raman memory are proposed in Chapter 4 offering the ability to demonstrate temporal multiplexing and deliver new technologies within photonic QIP.

In summary this thesis has has compared the breadth of the field of quantum memories and identified the Raman memory as having significant promise as a quantum memory, particularly within temporal multiplexing. It then presented simulation results, which indicate that the proposed noise-suppression method could enable the memory to operate at the single photon level and detailed the experimental requirements to investigate it. This has paved the way for the memory to develop and allow photonic networks and experiments to grow to unprecedented sizes.

Bibliography

[1] F. Jelezko, T. Ladd, R. Laflamme, C. Monroe, Y. Nakamura, and J. OBrien, "Quantum computers," *Nature*, vol. 464, 2010.

[2] L.-m. Duan, M. Lukin, J. Cirac, and P. Zoller, "Long-distance quantum communication with atomic ensembles and linear optics," *Nature*, vol. 414, no. 6862, pp. 413–418, 2001.

[3] F. Bussières, N. Sangouard, M. Afzelius, H. de Riedmatten, C. Simon, and W. Tittel, "Prospective applications of optical quantum memories," *Journal of Modern Optics*, vol. 60, no. 18, pp. 1519–1537, 2013.

[4] A. I. Lvovsky, B. C. Sanders, and W. Tittel, "Optical quantum memory," *Nature photonics*, vol. 3, no. 12, pp. 706–714, 2009.

[5] J. Nunn, I. Walmsley, M. Raymer, K. Surmacz, F. Waldermann, Z. Wang, and D. Jaksch, "Mapping broadband single-photon wave packets into an atomic memory," *Physical Review A*, vol. 75, no. 1, p. 011401, 2007.

[6] J. Nunn, N. Langford, W. Kolthammer, T. Champion, M. Sprague, P. Michelberger, X.-M. Jin, D. England, and I. Walmsley, "Enhancing multiphoton rates with quantum memories," *Physical review letters*, vol. 110, no. 13, p. 133601, 2013.

[7] P. S. Michelberger, T. F. M. Champion, M. R. Sprague, K. T. Kaczmarek, M. Barbieri, X. M. Jin, D. G. England, W. S. Kolthammer, D. J. Saunders, J. Nunn, and I. A. Walmsley, "Interfacing ghz-bandwidth heralded single photons with a warm vapour raman memory," *New Journal of Physics*, vol. 17, no. 4, p. 043006, 2015.

[8] M. Hosseini, G. Campbell, B. M. Sparkes, P. K. Lam, and B. C. Buchler, "Unconditional room-temperature quantum memory," *Nat Phys*, vol. 7, pp. 794–798, Oct 2011.

[9] H. Jeong, T. C. Ralph, and W. P. Bowen, "Quantum and classical fidelities for gaussian states," *JOSA B*, vol. 24, no. 2, pp. 355–362, 2007.

[10] S. Massar and S. Popescu, "Optimal extraction of information from finite quantum ensembles," *Physical review letters*, vol. 74, no. 8, p. 1259, 1995.

[11] C. Hong, Z.-Y. Ou, and L. Mandel, "Measurement of subpicosecond time intervals between two photons by interference," *Physical review letters*, vol. 59, no. 18, p. 2044, 1987.

[12] E. Knill, R. Laflamme, and G. J. Milburn, "A scheme for efficient quantum computation with linear optics," *Nature*, vol. 409, pp. 46–52, Jan. 2001.

[13] N. Sangouard, C. Simon, J. Minář, H. Zbinden, H. De Riedmatten, and N. Gisin, "Long-distance entanglement distribution with single-photon sources," *Physical Review A*, vol. 76, no. 5, p. 050301, 2007.

[14] H.-J. Briegel, W. Dür, J. I. Cirac, and P. Zoller, "Quantum repeaters: the role of imperfect local operations in quantum communication," *Physical Review Letters*, vol. 81, no. 26, p. 5932, 1998.

[15] S. Zaiser, T. Rendler, I. Jakobi, T. Wolf, S.-Y. Lee, S. Wagner, V. Bergholm, T. Schulte-Herbrüggen, P. Neumann, and J. Wrachtrup, "Enhancing quantum sensing sensitivity by a quantum memory," *Nature communications*, vol. 7, 2016.

[16] T. Pittman, B. Jacobs, and J. Franson, "Single photons on pseudodemand from stored parametric down-conversion," *Physical Review A*, vol. 66, no. 4, p. 042303, 2002.

[17] C. Xiong, X. Zhang, Z. Liu, M. Collins, A. Mahendra, L. Helt, M. Steel, D.-Y. Choi, C. Chae, P. Leong, *et al.*, "Active temporal multiplexing of indistinguishable heralded single photons," *Nature communications*, vol. 7, 2016.

[18] Y. Shih, "Entangled biphoton source-property and preparation," *Reports on Progress in Physics*, vol. 66, no. 6, p. 1009, 2003.

[19] A. Ling, A. Lamas-Linares, and C. Kurtsiefer, "Absolute emission rates of spontaneous parametric down-conversion into single transverse gaussian modes," *Physical Review A*, vol. 77, no. 4, p. 043834, 2008.

[20] H. J. Kimble, "The quantum internet," *Nature*, vol. 453, pp. 1023–1030, Jun 2008.

[21] T. Pittman and J. Franson, "Cyclical quantum memory for photonic qubits," *Physical Review A*, vol. 66, no. 6, p. 062302, 2002.

[22] P. M. Leung and T. C. Ralph, "Quantum memory scheme based on optical fibers and cavities," *Physical Review A*, vol. 74, no. 2, p. 022311, 2006.

[23] T. F. M. Champion, *"Towards storage and retrieval of non-classical light in a broadband quantum memory - An investigation of free-space and cavity Raman memories"*. PhD thesis, University of Oxford, 2015.

[24] F. Kaneda, F. Xu, J. Chapman, and P. G. Kwiat, "Quantum-memory-assisted multi-photon generation for efficient quantum information processing," *Optica*, vol. 4, no. 9, pp. 1034–1037, 2017.

[25] C. Langer, R. Ozeri, J. D. Jost, J. Chiaverini, B. DeMarco, A. Ben-Kish, R. Blakestad, J. Britton, D. Hume, W. M. Itano, *et al.*, "Long-lived qubit memory using atomic ions," *Physical Review Letters*, vol. 95, no. 6, p. 060502, 2005.

[26] M. Fleischhauer, A. Imamoglu, and J. P. Marangos, "Electromagnetically induced transparency: Optics in coherent media," *Reviews of modern physics*, vol. 77, no. 2, p. 633, 2005.

[27] S. Thomas, *"High Efficiency Broadband Raman Memory in Warm Caesium Vapour using Quenching,"* Master's thesis, Imperial College London, 2015.

[28] M. Fleischhauer and M. D. Lukin, "Dark-state polaritons in electromagnetically induced transparency," *Physical Review Letters*, vol. 84, no. 22, p. 5094, 2000.

[29] D. Phillips, A. Fleischhauer, A. Mair, R. Walsworth, and M. D. Lukin, "Storage of light in atomic vapor," *Physical Review Letters*, vol. 86, no. 5, p. 783, 2001.

[30] J. Cviklinski, J. Ortalo, J. Laurat, A. Bramati, M. Pinard, and E. Giacobino, "Reversible quantum interface for tunable single-sideband modulation," *Physical review letters*, vol. 101, no. 13, p. 133601, 2008.

[31] A. Turukhin, V. Sudarshanam, M. Shahriar, J. Musser, B. Ham, and P. Hemmer, "Observation of ultraslow and stored light pulses in a solid," *Physical Review Letters*, vol. 88, no. 2, p. 023602, 2001.

[32] L. Ma, O. Slattery, and X. Tang, "Optical quantum memory based on electromagnetically induced transparency," *Journal of Optics*, vol. 19, no. 4, p. 043001, 2017.

[33] A. Nicolas, L. Veissier, L. Giner, E. Giacobino, D. Maxein, and J. Laurat, "A quantum memory for orbital angular momentum photonic qubits," *Nature Photonics*, vol. 8, no. 3, pp. 234–238, 2014.

[34] V. Parigi, V. DAmbrosio, C. Arnold, L. Marrucci, F. Sciarrino, and J. Laurat, "Storage and retrieval of vector beams of light in a multiple-degree-of-freedom quantum memory," *Nature communications*, vol. 6, 2015.

[35] J. Nunn, *"Quantum Memory in Atomic Ensembles"*. PhD thesis, University of Oxford, 2008.

[36] K. Reim, J. Nunn, V. Lorenz, B. Sussman, K. Lee, N. Langford, D. Jaksch, and I. Walmsley, "Towards high-speed optical quantum memories," *Nature Photonics*, vol. 4, no. 4, pp. 218–221, 2010.

[37] P. J. Bustard, R. Lausten, D. G. England, and B. J. Sussman, "Toward quantum processing in molecules: A thz-bandwidth coherent memory for light," *Physical review letters*, vol. 111, no. 8, p. 083901, 2013.

[38] D. England, P. Bustard, J. Nunn, R. Lausten, and B. Sussman, "From photons to phonons and back: a thz optical memory in diamond," *Physical review letters*, vol. 111, no. 24, p. 243601, 2013.

[39] D.-S. Ding, W. Zhang, Z.-Y. Zhou, S. Shi, B.-S. Shi, and G.-C. Guo, "Raman quantum memory of photonic polarized entanglement," *Nature Photonics*, vol. 9, no. 5, pp. 332–338, 2015.

[40] E. L. Hahn, "Spin echoes," *Physical review*, vol. 80, no. 4, p. 580, 1950.

[41] N. Ohlsson, R. K. Mohan, and S. Kröll, "Quantum computer hardware based on rare-earth-ion-doped inorganic crystals," *Optics communications*, vol. 201, no. 1, pp. 71–77, 2002.

[42] N. Sangouard, C. Simon, H. De Riedmatten, and N. Gisin, "Quantum repeaters based on atomic ensembles and linear optics," *Reviews of Modern Physics*, vol. 83, no. 1, p. 33, 2011.

[43] K. F. Reim, P. Michelberger, K. C. Lee, J. Nunn, N. K. Langford, and I. A. Walmsley, "Single-photon-level memory at room temperature," in *Quantum Electronics and Laser Science Conference*, p. QThJ1, Optical Society of America, 2011.

[44] M. Eisaman, A. André, F. Massou, M. Fleischhauer, *et al.*, "Electromagnetically induced transparency with tunable single-photon pulses," *Nature*, vol. 438, no. 7069, p. 837, 2005.

[45] M. Namazi, C. Kupchak, B. Jordaan, R. Shahrokhshahi, and E. Figueroa, "Ultralow-noise room-temperature quantum memory for polarization qubits," 2017. To appear in *Physical Review Applied*.

[46] B. Lauritzen, J. Minář, H. De Riedmatten, M. Afzelius, N. Sangouard, C. Simon, and N. Gisin, "Telecommunication-wavelength solid-state memory at the single photon level," *Physical review letters*, vol. 104, no. 8, p. 080502, 2010.

[47] W. Rosenfeld, F. Hocke, F. Henkel, M. Krug, J. Volz, M. Weber, and H. Weinfurter, "Towards long-distance atom-photon entanglement," *Physical review letters*, vol. 101, no. 26, p. 260403, 2008.

[48] E. Distante, P. Farrera, A. Padrón-Brito, D. Paredes-Barato, G. Heinze, and H. De Riedmatten, "Storing single photons emitted by a quantum memory on a highly excited rydberg state," *Nature communications*, vol. 8, p. 14072, 2017.

[49] D. G. England, K. A. Fisher, J.-P. W. MacLean, P. J. Bustard, R. Lausten, K. J. Resch, and B. J. Sussman, "Storage and retrieval of thz-bandwidth single photons using a room-temperature diamond quantum memory," *Physical review letters*, vol. 114, no. 5, p. 053602, 2015.

[50] A. Seri, A. Lenhard, D. Rieländer, M. Gündoğan, P. M. Ledingham, M. Mazzera, and H. de Riedmatten, "Quantum correlations between single telecom photons and a multimode on-demand solid-state quantum memory," *Physical Review X*, vol. 7, no. 2, p. 021028, 2017.

[51] Y.-W. Cho, G. Campbell, J. Everett, J. Bernu, D. Higginbottom, M. Cao, J. Geng, N. Robins, P. Lam, and B. Buchler, "Highly efficient optical quantum memory with long coherence time in cold atoms," *Optica*, vol. 3, no. 1, pp. 100–107, 2016.

[52] J. Nunn, J. H. D. Munns, S. Thomas, K. T. Kaczmarek, C. Qiu, A. Feizpour, E. Poem, B. Brecht, D. J. Saunders, P. M. Ledingham, D. V. Reddy, M. G. Raymer, and I. A. Walmsley, "Theory of noise suppression in Λ-type quantum memories by means of a cavity," *Phys. Rev. A*, vol. 96, p. 012338, Jul 2017.

[53] D. Saunders, J. Munns, T. Champion, C. Qiu, K. Kaczmarek, E. Poem, P. Ledingham, I. Walmsley, and J. Nunn, "Cavity-enhanced room-temperature broadband raman memory," *Physical review letters*, vol. 116, no. 9, p. 090501, 2016.

[54] G. Romanov, C. OBrien, and I. Novikova, "Suppression of the four-wave mixing amplification via raman absorption," *Journal of Modern Optics*, vol. 63, no. 20, pp. 2048–2057, 2016.

[55] M. Hazewinkel, *Runge-Kutta Method.* Encyclopaedia of Mathematics; Springer / Kluwer Academic Publishers 1995.

[56] M. Hazewinkel, *Chebyshev Iteration Method.* Encyclopaedia of Mathematics; Springer / Kluwer Academic Publishers 1995.

[57] D. England, P. Michelberger, T. Champion, K. Reim, K. Lee, M. Sprague, X. Jin, N. Langford, W. Kolthammer, J. Nunn, *et al.*, "High-fidelity polarization storage in a gigahertz bandwidth quantum memory," *Journal of Physics B: Atomic, Molecular and Optical Physics*, vol. 45, no. 12, p. 124008, 2012.

[58] L. Essen and J. Parry, "An atomic standard of frequency and time interval: a caesium resonator," *Nature*, vol. 176, no. 4476, pp. 280–282, 1955.

[59] S. Thomas, J. Munns, K. Kaczmarek, C. Qiu, B. Brecht, A. Feizpour, P. Ledingham, I. Walmsley, J. Nunn, and D. Saunders, "High efficiency raman memory by suppressing radiation trapping," *New Journal of Physics*, vol. 19, no. 6, 2017.

[60] J. Borregaard, M. Zugenmaier, J. M. Petersen, H. Shen, G. Vasilakis, K. Jensen, E. S. Polzik, and A. S. Sørensen, "Scalable photonic network architecture based on motional averaging in room temperature gas," *Nature communications*, vol. 7, 2016.

[61] J. J. Abbott, "Parametric design of tri-axial nested helmholtz coils," *Review of Scientific Instruments*, vol. 86, no. 5, p. 054701, 2015.

[62] C. Santori, D. Fattal, J. Vuckovic, G. S. Solomon, and Y. Yamamoto, "Indistinguishable photons from a single-photon device," *nature*, vol. 419, no. 6907, p. 594, 2002.

[63] P. Chen, C. Shu, X. Guo, M. Loy, and S. Du, "Measuring the biphoton temporal wave function with polarization-dependent and time-resolved two-photon interference," *Physical review letters*, vol. 114, no. 1, p. 010401, 2015.

[64] B. Brecht, D. V. Reddy, C. Silberhorn, and M. Raymer, "Photon temporal modes: a complete framework for quantum information science," *Physical Review X*, vol. 5, no. 4, p. 041017, 2015.

Appendix A

Equations of Motion Derivation

A.1 Before Wave Propagation

Beginning with equations 2.15 - 2.19 and assuming (1) imperfect pumping to the ground state $|1\rangle$ such that $\hat{\sigma}_{11} = (1 - \alpha)$ and $\hat{\sigma}_{33} = \alpha$ and (2) the populations remain unchanged during the interaction $(\partial_t \hat{\sigma}_{ii} = 0)$ results in the following equations:

$$\partial_t \hat{\sigma}_{12} = i\omega_{21}\hat{\sigma}_{12} - i\hat{\mathbf{E}} \cdot [\mathbf{d}_{12}^*(1 - \alpha) + \mathbf{d}_{23}\hat{\sigma}_{13}] \tag{A.1}$$

$$\partial_t \hat{\sigma}_{23} = i\omega_{32}\hat{\sigma}_{23} + i\hat{\mathbf{E}} \cdot [\mathbf{d}_{23}^*\alpha + \mathbf{d}_{12}\hat{\sigma}_{13}] \tag{A.2}$$

$$\partial_t \hat{\sigma}_{13} = i\omega_{31}\hat{\sigma}_{13} - i\hat{\mathbf{E}} \cdot [\mathbf{d}_{23}^*\hat{\sigma}_{12} - \mathbf{d}_{12}^*\hat{\sigma}_{23}] \tag{A.3}$$

Transform into a rotating frame such that $\tilde{\sigma}_{jk} = \hat{\sigma}_{jk}e^{i\omega_{jk}\tau}$ where $\tau = t - z/c$.

$$\partial_t \tilde{\sigma}_{12} = -i\hat{\mathbf{E}} \cdot [\mathbf{d}_{12}^*(1 - \alpha)e^{-i\omega_{21}\tau} + \mathbf{d}_{23}\tilde{\sigma}_{13}e^{-i\omega_{23}\tau}] \tag{A.4}$$

$$\partial_t \tilde{\sigma}_{23} = +i\hat{\mathbf{E}} \cdot (\mathbf{d}_{23}^*\alpha e^{i\omega_{23}\tau} + \mathbf{d}_{12}\tilde{\sigma}_{13}e^{i\omega_{21}\tau}) \tag{A.5}$$

$$\partial_t \tilde{\sigma}_{13} = -i\hat{\mathbf{E}} \cdot [\mathbf{d}_{23}^*\tilde{\sigma}_{12}e^{i\omega_{23}\tau} - \mathbf{d}_{12}^*\tilde{\sigma}_{23}e^{-i\omega_{21}\tau}] \tag{A.6}$$

The electric field operator is comprised of the 3 electric field equations defined by equations 2.10 - 2.10.

$$\mathbf{E_c}(z,t) = \mathbf{v_c}E_c(z,t)e^{i\omega_c\tau} + c.c. \tag{A.7}$$

$$\mathbf{E_s}(z,t) = i\mathbf{v_s}g_s\hat{S}(z,t)e^{i\omega_s\tau} + h.c. \tag{A.8}$$

$$\mathbf{E_a}(z,t) = i\mathbf{v_a}g_a\hat{A}(z,t)e^{i\omega_a\tau} + h.c. \tag{A.9}$$

Using the rotating wave approximation we can choose to keep frequencies which only are the difference of an $\mathbf{E}$ and a transition. Only keep terms rotating at a frequency difference e.g. $\omega_{21a} = (\omega_2 - \omega_1) - \omega_a$.

$$\begin{aligned} \partial_t \tilde{\sigma}_{12} = -i\,[\,(1-\alpha)\mathbf{d}_{12}^* \cdot (i\mathbf{v}_s g_s\hat{S}e^{-i\omega_{21s}\tau} &+ \mathbf{v}_c E_c e^{-i\omega_{21c}\tau} + i\mathbf{v}_a g_a\hat{A}e^{-i\omega_{21a}\tau}) \\ + \mathbf{d}_{23} \cdot \tilde{\sigma}_{13}(i\mathbf{v}_s g_s\hat{S}e^{-i\omega_{23s}\tau} &+ \mathbf{v}_c E_c e^{-i\omega_{23c}\tau} + i\mathbf{v}_a g_a\hat{A}e^{-i\omega_{23a}\tau})\,] \end{aligned} \tag{A.10}$$

$$\partial_t\tilde\sigma_{23} = -i\,[\,\mathbf{d}_{12}\cdot\tilde\sigma_{13}(i\mathbf{v}_s^*g_s\hat S^\dagger e^{i\omega_{21s}\tau} - \mathbf{v}_c^*E_c^*e^{i\omega_{21c}\tau} + i\mathbf{v}_a^*g_a\hat A^\dagger e^{i\omega_{21a}\tau})$$
$$-\alpha\mathbf{d}_{23}^*\cdot(-i\mathbf{v}_s^*g_s\hat S^\dagger e^{i\omega_{23s}\tau} + \mathbf{v}_c^*E_c^*e^{i\omega_{23c}\tau} - i\mathbf{v}_a^*g_a\hat A^\dagger e^{i\omega_{23a}\tau})\,] \tag{A.11}$$

$$\partial_t\tilde\sigma_{13} = i\left[\mathbf{d}_{12}^*\cdot\tilde\sigma_{23}(i\mathbf{v}_sg_s\hat S e^{-i\omega_{21s}\tau} + \mathbf{v}_cE_ce^{-i\omega_{21c}\tau} + i\mathbf{v}_ag_a\hat A e^{-i\omega_{21a}\tau})\right.$$
$$\left.-\mathbf{d}_{23}^*\cdot\tilde\sigma_{12}(-i\mathbf{v}_s^*g_s\hat S^\dagger e^{i\omega_{23s}\tau} + \mathbf{v}_c^*E_c^*e^{i\omega_{23c}\tau} - i\mathbf{v}_a^*g_a\hat A^\dagger e^{i\omega_{23a}\tau})\right] \tag{A.12}$$

Defining blue detuning as positive, i.e $\omega_{23a} = (\omega_2 - \omega_3) - \omega_a = -\Delta_a$ and the ground state splitting as ω_b:

$$\partial_t\tilde\sigma_{12} = -i\left[(1-\alpha)\mathbf{d}_{12}^*\cdot(i\mathbf{v}_sg_s\hat S e^{i\Delta_s\tau} + \mathbf{v}_cE_ce^{i(\Delta_s+\omega_b)\tau} + i\mathbf{v}_ag_a\hat A e^{i(\Delta_s+2\omega_b)\tau})\right.$$
$$\left.+\mathbf{d}_{23}\cdot\tilde\sigma_{13}(i\mathbf{v}_sg_s\hat S e^{i(\Delta_s-\omega_b)\tau} + \mathbf{v}_cE_ce^{i(\Delta_a-\omega_b)\tau} + i\mathbf{v}_ag_a\hat A e^{i\Delta_a\tau})\right] \tag{A.13}$$

$$\partial_t\tilde\sigma_{23} = -i\,[\,\mathbf{d}_{12}\cdot\tilde\sigma_{13}(i\mathbf{v}_s^*g_s\hat S^\dagger e^{-i\Delta_s\tau} - \mathbf{v}_c^*E_c^*e^{-i(\Delta_s+\omega_b)\tau} + i\mathbf{v}_a^*g_a\hat A^\dagger e^{-i(\Delta_s+2\omega_b)\tau})$$
$$-\alpha\mathbf{d}_{23}^*\cdot(-i\mathbf{v}_s^*g_s\hat S^\dagger e^{-i(\Delta_s-\omega_b)\tau} + \mathbf{v}_c^*E_c^*e^{-i(\Delta_a-\omega_b)\tau} - i\mathbf{v}_a^*g_a\hat A^\dagger e^{-i\Delta_a\tau})\,] \tag{A.14}$$

$$\partial_t\tilde\sigma_{13} = i\left[\mathbf{d}_{12}^*\cdot\tilde\sigma_{23}(i\mathbf{v}_sg_s\hat S e^{i\Delta_s\tau} + \mathbf{v}_cE_ce^{i(\Delta_s+\omega_b)\tau} + i\mathbf{v}_ag_a\hat A e^{i(\Delta_s+2\omega_b)\tau})\right.$$
$$\left.-\mathbf{d}_{23}^*\cdot\tilde\sigma_{12}(-i\mathbf{v}_s^*g_s\hat S^\dagger e^{-i(\Delta_s-\omega_b)\tau} + \mathbf{v}_c^*E_c^*e^{-i(\Delta_a-\omega_b)\tau} - i\mathbf{v}_a^*g_a\hat A^\dagger e^{-i\Delta_a\tau})\right] \tag{A.15}$$

Factorising sensibly and using $\Delta_a - \Delta_s = \omega_b$

$$\partial_t\tilde\sigma_{12} = -ie^{i\Delta_s\tau}\left[(1-\alpha)\mathbf{d}_{12}^*\cdot(i\mathbf{v}_sg_s\hat S + \mathbf{v}_cE_ce^{i\omega_b\tau} + i\mathbf{v}_ag_a\hat A e^{2i\omega_b\tau})\right.$$
$$\left.+\mathbf{d}_{23}\cdot\tilde\sigma_{13}(i\mathbf{v}_sg_s\hat S e^{-i\omega_b\tau} + \mathbf{v}_cE_c + i\mathbf{v}_ag_a\hat A e^{i\omega_b\tau})\right] \tag{A.16}$$

$$\partial_t\tilde\sigma_{23} = -ie^{-i\Delta_a\tau}\,[\,\mathbf{d}_{12}\cdot\tilde\sigma_{13}(i\mathbf{v}_s^*g_s\hat S^\dagger e^{i\omega_b\tau} - \mathbf{v}_c^*E_c^* + i\mathbf{v}_a^*g_a\hat A^\dagger e^{-i\omega_b\tau})$$
$$-\alpha\mathbf{d}_{23}^*\cdot(-i\mathbf{v}_s^*g_s\hat S^\dagger e^{2i\omega_b\tau} + \mathbf{v}_c^*E_c^*e^{i\omega_b\tau} - i\mathbf{v}_a^*g_a\hat A^\dagger)\,] \tag{A.17}$$

$$\partial_t\tilde\sigma_{13} = i\,[\,\mathbf{d}_{12}^*\cdot\tilde\sigma_{23}e^{i\Delta_a\tau}(i\mathbf{v}_sg_s\hat S e^{-i\omega_b\tau} + \mathbf{v}_cE_c + i\mathbf{v}_ag_a\hat A e^{i\omega_b\tau})$$
$$-\mathbf{d}_{23}^*\cdot\tilde\sigma_{12}e^{-i\Delta_s\tau}(-i\mathbf{v}_s^*g_s\hat S^\dagger e^{i\omega_b\tau} + \mathbf{v}_c^*E_c^* - i\mathbf{v}_a^*g_a\hat A^\dagger e^{-i\omega_b\tau})\,] \tag{A.18}$$

A.2   After Wave Propagation

Subbing in definitions for P, R and $\hat B$ in 2.30 - 2.32 we find $\tilde{\mathbf{P}}_s = \sqrt{n}\mathbf{d}_{12}P$ and $\tilde{\mathbf{R}}_s^\dagger = \sqrt{n}\mathbf{d}_{23}R^\dagger$. Adding phonological decay rates $\gamma_{s,a}$ for P and $R^\dagger$ we yields:

$$\left(\frac{i}{2k_s}\nabla_\perp^2 + \partial_z + \frac{1}{c}\partial_t\right)\hat S = -\chi_s^{*(12)}P \tag{A.19}$$

$$\left(\frac{i}{2k_a}\nabla_\perp^2 + \partial_z + \frac{1}{c}\partial_t\right)\hat A = -\chi_a^{*(23)}R^\dagger \tag{A.20}$$

$$\partial_t P = [(1-\alpha)(\chi_s^{(12)}\hat{S} - i\Omega_{12}^* e^{i\omega_b\tau} + \chi_a^{(12)}\hat{A}e^{2i\omega_b\tau}) + \chi_s^{(23)}\hat{B}\hat{S}e^{-i\omega_b\tau} - i\Omega_{23}\hat{B} + \chi_a^{(23)}\hat{B}\hat{A}e^{i\omega_b\tau}\,]$$
$$- (i\Delta_s + \gamma_s)P \tag{A.21}$$

$$\partial_t R^\dagger = [\chi_s^{(12)}\hat{B}\hat{S}^\dagger e^{i\omega_b\tau} + i\Omega_{12}\hat{B} + \chi_a^{(12)}\hat{B}\hat{A}^\dagger e^{-i\omega_b\tau} + \alpha(\chi_s^{*(23)}\hat{S}^\dagger e^{2i\omega_b\tau} + i\Omega_{23}^* e^{i\omega_b\tau} + \chi_a^{*(23)}\hat{A}^\dagger)\,]$$
$$- (-i\Delta_a + \gamma_a)R^\dagger \tag{A.22}$$

$$\partial_t \hat{B} = [(-\chi_s^{*(12)}\hat{S}e^{-i\omega_b\tau} + i\Omega_{12}^* - \chi_a^{*(12)}\hat{A}e^{i\omega_b\tau})R^\dagger$$
$$- (\chi_s^{*(23)}\hat{S}^\dagger e^{i\omega_b\tau} + i\Omega_{23}^* + \chi_a^{*(23)}\hat{A}^\dagger e^{-i\omega_b\tau})P\,] \tag{A.23}$$

where the Rabi frequencies are defined as $\Omega_{23} = \frac{\mathbf{d}_{23}\cdot\mathbf{v}_c}{\hbar}E_c$ and $\Omega_{12} = \frac{\mathbf{d}_{12}\cdot\mathbf{v}_c^*}{\hbar}E_c^*$. The coupling constants χ_s and χ_a are given by:

$$\chi_s^{(ij)} = \frac{\mathbf{d}_{ij}\cdot\mathbf{v}_s^*}{\hbar}\sqrt{n}g_s = \frac{\mathbf{d}_{ij}\cdot\mathbf{v}_s}{\hbar}\sqrt{\frac{\hbar\omega_s n}{2\epsilon_0 c}} \tag{A.24}$$

$$\chi_a^{(ij)} = \frac{\mathbf{d}_{ij}\cdot\mathbf{v}_a^*}{\hbar}\sqrt{n}g_a = \frac{\mathbf{d}_{ij}\cdot\mathbf{v}_a}{\hbar}\sqrt{\frac{\hbar\omega_a n}{2\epsilon_0 c}} \tag{A.25}$$

Now, assuming the only time dependencies are the ones explicit in exponentials which follows from the adiabatic approximation. We may also assume that the annihilation and creation operators $(\hat{S}, \hat{A}, \hat{B})$ are small (order ϵ) and hence neglect product terms. Solve $\partial_t P$ & $\partial_t R^\dagger$, defining $\Gamma_{s,a} = \gamma_{s,a} + i\Delta_{s,a}$

$$P = (1-\alpha)\left(\frac{\chi_s^{(12)}}{\Gamma_s}\hat{S}\epsilon - \frac{i\Omega_{12}^* e^{i\omega_b\tau}}{\Gamma_a} + \frac{\chi_a^{(12)} e^{2i\omega_b\tau}}{\Gamma_a + i\omega_b}\hat{A}\epsilon\right) - \frac{i\Omega_{23}}{\Gamma_s}\hat{B}\epsilon + c_1 e^{-\Gamma_s\tau} \tag{A.26}$$

$$R^\dagger = \frac{i\Omega_{12}}{\Gamma_a^*}\hat{B}\epsilon + \alpha\left(\frac{\chi_s^{*(23)} e^{2i\omega_b\tau}}{\Gamma_s^* + i\omega_b}\hat{S}^\dagger\epsilon + \frac{i\Omega_{23}^* e^{i\omega_b\tau}}{\Gamma_s^*} + \frac{\chi_a^{*(23)}}{\Gamma_a^*}\hat{A}^\dagger\epsilon\right) + c_2 e^{-\Gamma_a^*\tau} \tag{A.27}$$

The adiabatic approximation allows the $e^{-\Gamma\tau}$ terms to be neglected. Sub in P and $R^\dagger$ into $\partial_t B$.

$$\partial_t \hat{B} = (-\chi_s^{*(12)}\hat{S}\epsilon e^{-i\omega_b\tau} + i\Omega_{12}^* - \chi_a^{*(12)}\hat{A}\epsilon e^{i\omega_b\tau})\left(\frac{i\Omega_{12}}{\Gamma_a^*}\hat{B}\epsilon + \alpha\left(\frac{\chi_s^{*(23)} e^{2i\omega_b\tau}}{\Gamma_s^* + i\omega_b}\hat{S}^\dagger\epsilon + \frac{i\Omega_{23}^* e^{i\omega_b\tau}}{\Gamma_s^*} + \frac{\chi_a^{*(23)}}{\Gamma_a^*}\hat{A}^\dagger\epsilon\right)\right)$$
$$- (\chi_s^{*(23)}\hat{S}^\dagger\epsilon e^{i\omega_b\tau} + i\Omega_{23}^* + \chi_a^{*(23)}\hat{A}^\dagger\epsilon e^{-i\omega_b\tau})\left[(1-\alpha)\left(\frac{\chi_s^{(12)}}{\Gamma_s}\hat{S}\epsilon - \frac{i\Omega_{12}^* e^{i\omega_b\tau}}{\Gamma_a} + \frac{\chi_a^{(12)} e^{2i\omega_b\tau}}{\Gamma_a + i\omega_b}\hat{A}\epsilon\right) - \frac{i\Omega_{23}}{\Gamma_s}\hat{B}\epsilon\right] \tag{A.28}$$

The rotating wave approximation means only terms which product to stationary are kept, as well as neglecting higher order terms in ϵ. This results in the following equation for $\partial_t \hat{B}$:

$$\partial_t \hat{B} = -i\Omega^*_{23} \left[(1-\alpha)\frac{\chi_s^{(12)}}{\Gamma_s} + \alpha\frac{\chi_s^{*(12)}}{\Gamma_s^*} \right] \hat{S} + i\Omega^*_{12} \left[(1-\alpha)\frac{\chi_a^{(23)}}{\Gamma_a} + \alpha\frac{\chi_a^{*(23)}}{\Gamma_a^*} \right] \hat{A}^\dagger$$
$$- \left[\frac{|\Omega_{12}|^2}{\Gamma_a^*} + \frac{|\Omega_{23}|^2}{\Gamma_s} \right] \hat{B} \tag{A.29}$$

Finally using the definition of optical depth $d = \frac{|\chi|^2 L}{\gamma}$ and using the equations for P and $R^\dagger$ in equations A.19 and A.20 whilst re-constraining to 1 spatial dimension (z) (assuming small divergence) we can write:

$$\partial_t \hat{B} = -i\Omega^*_{23}\sqrt{\frac{d\gamma_s}{L}} \left[\frac{(1-\alpha)}{\Gamma_s} + \frac{\alpha}{\Gamma_s^*} \right] \hat{S} + i\Omega^*_{12}\sqrt{\frac{d\gamma_a}{L}} \left[\frac{(1-\alpha)}{\Gamma_a} + \frac{\alpha}{\Gamma_a^*} \right] \hat{A}^\dagger$$
$$- \left[\frac{|\Omega_{12}|^2}{\Gamma_a^*} + \frac{|\Omega_{23}|^2}{\Gamma_s} \right] \hat{B} \tag{A.30}$$

$$(c\partial_z + \partial_t)\hat{S} = ic\sqrt{\frac{d\gamma_s}{L}}\frac{\Omega_{23}}{\Gamma_s}\hat{B} - \kappa_s\hat{S} \tag{A.31}$$

$$(c\partial_z + \partial_t)\hat{A} = ic\sqrt{\frac{d\gamma_a}{L}}\frac{\Omega_{12}}{\Gamma_a}\hat{B}^\dagger - \kappa_a\hat{A} \tag{A.32}$$

Where $\kappa_s = \frac{d\gamma_s}{\tau}\left[\frac{(1-\alpha)}{\Gamma_s} + \frac{\alpha}{\Gamma_s^*+i\omega_b}\right]$ and $\kappa_a = \frac{d\gamma_a}{\tau}\left[\frac{(1-\alpha)}{\Gamma_a+i\omega_b} - \frac{\alpha}{\Gamma_a^*}\right]$